TRANSITION TO TURBULENCE IN SHEAR-THINNING FLUIDS

A Dissertation

by

NI ZHEN

Submitted to the Office of Graduate and Professional Studies of
Texas A&M University
in partial fulfillment of the requirements for the degree of

DOCTOR OF PHILOSOPHY

Chair of Committee,	Robert Handler
Committee Members,	Kumbakonam Rajagopal
	Gerald Morrison
	Suhasini Subba Rao
Head of Department,	Andreas Polycarpou

May 2014

Major Subject: Mechanical Engineering

ABSTRACT

In this dissertation, the effects of a shear-thinning fluid on the evolution of a hairpin vortex are investigated. The fluid viscosity is determined using a power law model and direct numerical simulations are performed using a pseudo-spectral code. The Reynolds number is defined using the initial maximum velocity and the initial viscosity at the wall. In the simulations, the Reynolds number and the initial strength of the hairpin vortex are fixed. We observe from 3D visualizations that the hairpin tends to lose its coherence more easily and breaks into small scale structures when the level of shear thinning is increased. The disintegration of the hairpin causes a decrease in the production of kinetic energy and an increase in dissipation. As a consequence, the transition to turbulence is delayed as the level of shear thinning is increased. In future work, we will investigate the effects of shear-thinning on fully developed turbulence, and we will study the effects of other rheological models such as the Carreau model.

ACKNOWLEDGEMENTS

I would like to thank my parents for the generous financial support during the entire duration of my PhD program.

I also would like to thank my Ph.D. advisor Dr. Handler.

NOMENCLATURE

HP	hairpin
HPE	hairpin energy
DNS	direct numerical simulation
RCA	right coronary arteries
WSS	wall shear stress
Ω_z	vorticity in the z direction
t^*	time scale of dissipation due to viscosity
u_i	total velocity
u	total velocity in the x direction
v	total velocity in the y direction
w	total velocity in the z direction
p	pressure divided by density
T_{ji}	viscous stress tensor divided by the density
f_x	constant driving pressure gradient in the x direction
S_{ji}	symmetric part of the velocity gradient tensor
ν	kinematic viscosity
K	fluid consistency divided by density
n	power law index
L_x	domain length in the x direction

L_y	domain length in the y direction
L_z	domain length in the z direction
D	height of the half channel
$\vec{V}_{hp}$	velocity field of the mature hairpin
U_{hp}	hairpin velocity in the x direction
V_{hp}	hairpin velocity in the y direction
W_{hp}	hairpin velocity in the z direction
u_{rand}	spatially random flow field velocity in the x direction
v_{rand}	spatially random flow field velocity in the y direction
w_{rand}	spatially random flow field velocity in the z direction
$u_{th}(y)$	analytical solution for a steady laminar flow of a power law fluid in a half channel
ν_{th}	initial kinematic viscosity at the no-slip boundary
$\bar{}$	volumetric average
$\langle\ \rangle$	horizontal average
C_{hp}	constant which sets the amplitude of the initial strength of the hairpin vortex
C_{rand}	constant used to vary the amplitude of a spatially random flow field

rms	root-mean-square velocity
Re	Reynolds number defined using the initial velocity at the shear free boundary
Re^*	friction Reynolds number
u^*	friction velocity
τ	shear stress at the no-slip boundary
λ_2	eigenvalue of the sum of the squares of the rate of strain tensor and the rotation tensor
u_j'	fluctuating velocity
k	volumetric average of the kinetic energy of the fluctuations
P_1	volumetric average of the production of turbulence due to shear
P_2	volumetric average of the production of turbulence due to non-Newtonian effects
γ	volumetric average of the dissipation
β_{ij}	fluctuating part of the symmetric part of the velocity gradient tensor
Ω_{ji}'	fluctuating part of the anti-symmetric part of the velocity gradient tensor
t	time

TABLE OF CONTENTS

Page

LIST OF FIGURES

LIST OF TABLES

TABLE Page

1. INTRODUCTION

1.1 Literature Survey

Shear-thinning substances, which are common in nature and are used in products encountered in daily life, are those whose viscosity decreases with increasing flow rate. Many of these substances behave like solids or highly viscous liquids at low shear rates but flow more readily at higher rates of shear. Shear-thinning substances encountered in daily life are numerous and common and include milk, greases, waxes, paints, mud, ketchup, mayonnaise, printing ink, paper coatings, toothpaste, and crude oil (Mewis, 1979; Verreet and Berlamont, 1988; Dickie and Kokini, 1983; Chhabra and Richardson, 1999; Hieber and Shen, 1980; Ikoku and Ramey, 1979). Many fluids of biological origin such as blood, mucous, chyme, and synovial fluid are also shear-thinning (Johnston et al., 2004; Raju and Devanathan, 1974; Srivastava and Srivastava, 1985). Their ubiquity leads to their inevitable importance in a wide variety of applications including those in oil recovery (Ikoku and Ramey, 1979; Veatch, 1983), food processing (Dickie, 1983), lubrication (Sinha et al., 1983; Bhattacharjee and Das, 1996), biological fluid mechanics (Johnston et al., 2004), construction where ceramics, cement and concrete are shear-thinning (Mewis, 1979), and in nuclear power generation where molten salts are shear-thinning (Mewis, 1979). In oil recovery, particular in the hydraulic fracturing operation, polymer is injected in water. Water then becomes shear-thinning. Here we want to distinguish fluids which are purely shear-thinning from other non-Newtonian fluids

which may also exhibit elasticity. These fluids, which will not be addressed in this dissertation, include high molecular weight polymer solutions (Lumley, 1969; Lumley, 1973; Sureshkumar et al., 1997).

The original definition of thixotropy referred to an isothermal, reversible, solid liquid transformation caused by mechanical agitation (Mewis, 1979). Currently, the general definition of thixotropy is the decrease of apparent viscosity due to shear over time and the recovery of viscosity when the flow rate is reduced. Neither shear-thinning nor elastic effects are excluded in this definition. However, the time scale of thixotropy is not the same as the time scale of viscoelastic relaxation. The time-dependent behavior of thixotropy instead of viscoelasticity is investigated. The list of all thixotropic materials is impossible to compose. Instead, they can be classified in groups based upon their origins or applications. In the field of rheology, thixotropy seems to be one of the most neglected areas despite the importance of thixotropic materials in industrial and scientific applications.

The human body is a thermal hydraulic system and the heart is the pump. Coronary heart disease is one of the important causes of death in the Western World (Johnston et al., 2004). The WSS distribution in coronary arteries is considered to be a major contributing factor to the initial symptoms of this disease. Steady state simulations of blood flow in human RCA were performed using five non-Newtonian blood models and the Newtonian model. For the blood viscosity, in regions of mid to high shear, Newtonian model is a good approximation while in regions of low shear, Generalized Power Law model is more suitable. This model tends to the Newtonian model in regions

of mid to high shear. There is significant variation in the geometry of RCA. These geometric differences can cause considerable variations in arterial flow patterns and therefore the distribution of WSS. In general, WSS was observed to be lower at the entrance to the artery than the end of the section simulated. For low velocities, the non-Newtonian aspect of blood flow in the RCA is significant. The relationships between radius, curvature and WSS require further investigation.

Drag reduction by additives was studied by Lumley (1969). It was observed by Toms (1948) the addition of polymethylmethacrylate to high-Reynolds number turbulent pipe flow of monochlorobenzene caused significantly reduction of pressure drop versus the solvent alone at the same flow rate. The definition of drag reduction is the decrease of skin friction in turbulent flow lower than that of the solvent alone. This definition allows the investigators to focus on the effective additives. The definition of Newtonian is the proportionality of the extra-stress tensor and the strain-rate tensor for both steady and unsteady flows. Any departure will be classified as non-Newtonian behavior. Polymers with a linear structure while having minimum side chains are the most effective. Effectiveness was measured as the required concentration in order to produce a certain level of drag reduction. As the chain length increases, the effectiveness increases as well. When the polymer-solvent interactions are favored instead of the polymer-polymer interactions, the polymer is extended. Effectiveness increases as the chain expansion increases. There was no indication to suggest that molecular diameter is an important factor. In high concentrations, all the polymer-solvent combinations display drag reduction as well as viscoelastic effects. One example of these effects is the phase

difference between stress and strain rate in oscillatory Couette flow. For certain solutions such as Carbopol, viscoelastic effects are absent. It was observed that drag reduction is also absent in these solutions. Agglomerations of polymer molecules are formed and broken up by the fluctuating strain rate of the turbulence. It is unclear whether these agglomerations contribute to drag reduction. In the velocity profiles of the polymer-solvent flows, the logarithmic portion of the law of the wall is moved upward. The polymer flows are observed to form agglomerations in the size of the order of the dissipative scales. Detailed spectral measurements using device such as the laser-Doppler velocimeter should be made at dissipative scales.

The drag reduction in a pipe with the addition of polymer was investigated by Lumley (1973). When the wall shear stress is high enough, the fluctuating strain induces the molecules to expand which causes the increase of effective viscosity. The extent of expansion depends on the concentration. As a consequence, the intensity of the small eddies in the buffer layer is gradually reduced. The viscosity deep in the viscous sublayer is unaffected where the expansion of molecules is absent. Due to the reduced intensity of the small eddies, the decreased Reynolds stress at buffer layer delays the reduction of mean profile slope. As a result, the buffer zone between the viscous sublayer and the inertial sublayer is thickened. The large eddies which expand with the sublayer produce an increased streamwise fluctuating velocity from the mean velocity profile mainly in the buffer layer. For small concentration, the drag reduction seems to be proportional to the concentration. The maximum drag reduction asymptote corresponds to the viscous sublayer which reaches the center of the pipe. Analysis in

Newtonian boundary layers shows the small eddies outside the viscous sublayer instead of the large eddies transport most of the momentum normal to the wall. The large eddies produce an inflectionary mean velocity profile by sweeping slow-moving fluid up from the wall. Far from the viscous influence of the wall, this velocity profile becomes unstable and produces small eddies which are responsible for the Reynolds stress, in other words, the transport of the momentum. The behaviors of these eddies in a polymer solution were studied. The thickening of the sublayer produces an increase in the thickness and spacing of the large eddies. The dynamics of the growth and decay of the large eddies remain the same in a drag-reducing flow as in a Newtonian flow. Turbulence is primarily consisted of large eddies in the maximum drag-reduction regime.

Understanding wall-bounded turbulence is critical not only due to its fundamental importance in the theory of turbulence (Barenblatt et al., 1997) but also because of its obvious significance in determining skin friction drag on virtually all vehicles and devices which move relative to a fluid. Original theories of homogeneous turbulence were developed using statistical models (Batchelor, 1953; Lin, 1961; Taylor, 1935; von Karman, 1937) that treated turbulence as an agglomeration of interacting random 'eddies', which produce random vorticity and velocity fields. These ideas were challenged to some extent by Theodorsen (1952), who was the first to conjecture that wall-bounded turbulence may not be completely random in nature but might be composed of 'coherent' elements, which were termed 'horseshoe' vortices. These structures are thought to form when perturbed spanwise (cross-stream) vortex lines

associated with the mean flow would lift away from a no-slip boundary due to vortex self-induction. The ‘heads’ of these mini-horseshoe vortices would then, because of their location farther from the wall, move faster than their ‘tails’, thereby giving rise to stretching and amplification of the vorticity in their ‘legs’. Subsequent experimental and numerical investigations revealed considerable evidence for the existence of these structures and have shown that they indeed have a statistically significant signature (Kline et al., 1967; Smith and Metzler, 1983; Brooke and Hanratty, 1993; Bernard et al., 1993; Robinson, 1991; Adrian, 2007). Based on these and other similar investigations, the term ‘hairpin’ vortex has been used to characterize the typical structure found in wall-bounded turbulence. Hairpins are found to have ‘legs’, elongated streamwise oriented flow structures which are termed quasi-streamwise vortices. Hairpins can appear singly. They also regenerate themselves through naturally creating multiple, streamwise-organized hairpins. This remarkable regenerative property of hairpin vortices results in the spontaneous formation of clusters of such vortices which were termed ‘packets’ by Adrian. Packets of hairpins have long persistence. Quasi-streamwise vortices and the associated streaks of both high and low momentum are visible in the buffer layer. There is also evidence to suggest that they occur in the logarithmic layer and maybe even in the wake region. The hairpins are most frequently observed in the logarithmic layer and less seen with increasing distance from the wall. They sometimes penetrate the entire boundary layer and possibly form the source of turbulent bulges. The scale of the structures increases with distance from the wall. The growth of the packets transports vorticity, low momentum and turbulent kinetic energy from the wall. This

growth is not exclusively responsible for the transport since turbulence is also generated by gradients away from the wall. The relationship between the large scales of motion which support a significant fraction of the Reynolds stress and the turbulent kinetic energy and the hairpin packets are yet to be discovered for fully turbulent flows (Adrian, 2007). A particularly striking example of the regenerative property of hairpin vortices is found in the recent simulation of turbulent spots. In this DNS, turbulent spots were found to be composed of large clusters of hairpins or parts of hairpins (Strand and Goldstein, 2011). Hairpins may in some sense be thought of as the fundamental building block of wall-bounded turbulence. Large scale motions are macroscopic while hairpins are microscopic. We study the hairpins in order to understand its effects on macroscopic phenomena, for example, heat transfer. The convective heat transfer coefficients are affected by the flow regime.

The studies of turbulent boundary layers are presented by Kline et al (1967). The structure of any turbulent flow shows the local balance of production, transport and dissipation of turbulent kinetic energy. Within the so-called laminar sublayer, well-organized spatially and temporally dependent motions are present. In the region very near the wall, low-speed streaks are formed due to these motions. The interactions between the streaks and the outer portions of the flow follow a process of gradual lift-up, abrupt oscillation, bursting and ejection. These processes are critical in the production of new turbulence as well as the transport of turbulence within the boundary layer on smooth walls. Production plays a primary role in turbulent boundary layers and it is concentrated in the rather thin region very near the wall. The understanding of turbulent

structure in this region is particularly important. The structure of the entire boundary layer is determined predominantly by the thin wall region. Motions in the wall region are dominated by viscosity. However, eddy motions are present throughout the entire wall region. The violent ejection of low-speed fluid from the regions near the wall is primarily responsible for the production of turbulent kinetic energy in the inner region of the boundary layer. A positive pressure gradient intensifies the bursting. In certain accelerating flows, the bursting ceases entirely which causes the relaminarization of the boundary layer. Wall-layer streak breakup is important for the determination of the structure of the entire turbulent boundary layer. Wall-layer streaks are formed due to vortex stretching which is caused by large fluctuations which act on the flow near a smooth wall with a strong mean strain present. The production of turbulence near the wall originates from a local, short-lasting, on and off dynamic instability of the instantaneous velocity profile near the wall. This instability acts to maintain the mean flow. The ejection of fluid away from the wall is crucial for the transfer of energy, momentum and vorticity between the inner and outer regions. The outer regions are otherwise known as wake.

The evolution of a hairpin vortex for a Newtonian fluid in a low Reynolds number channel was studied using DNS (Zhou et al., 1999). Only when the strength of the initial structure reaches or surpasses a threshold can the autogeneration be possible. Due to the mutual induction process, in the long legs of the primary hairpin vortex, a kink forms. The shear layer between the long legs is the strongest near the kink. The long legs of the primary vortex are cut off near the kink when the shear layer rolls-up and turns into a

spanwise vortex. This vortex connects viscously with the upstream sections of the legs and forms the secondary hairpin vortex which is detached from the legs of the primary hairpin vortex. Hairpins with stronger initial strength generate new hairpins more quickly than the weaker ones. The results suggest the existence of an optimal distance of the initial structure from the wall due to the competing effects of self as well as mutual induction and the vortex stretching in the streamwise direction by the mean shear. Apart from the secondary and tertiary vortices, new hairpins also emerge on the downstream side of the primary hairpin vortex. The downstream vortices grow out of a pair of quasi-streamwise vertical tongues that stick out from the head of the primary hairpin on the downstream side. This pair of tongues evolves into a second downstream hairpin vortex. This process results in the generation of several downstream hairpin vortices in quick succession. Most of these hairpins are not strong enough and experience rapid decay. With the introduction of asymmetry, the simulation results compare better with the experiments. Experimental evidence shows that quasi-streamwise vortices occur singly usually and counter-rotating pairs of equal strength are rarely observed. The simulation results suggest that the influence of local spanwise velocity can be the cause of the experimentally observed asymmetry. The asymmetry aids in the subsequent formation of new hairpins. The initial threshold for the autogeneration becomes lower with the introduction of asymmetry. The simulation results indicate the coherent vortex packets are a fundamental flow feature of the near-wall region for a low Reynolds number. The authors believe this is also true for a high Reynolds number.

Purely shear-thinning have been found to play an important role not only in lower speed laminar flows, such as in lubrication applications and in biological flows, but also in higher speed, higher Reynolds number flows. In particular, they have been found recently to play a significant role in modifying the behavior of fully turbulent flows as well as in delaying the transition of laminar flows to fully turbulent ones. However, the details of how they affect complex flows such as those at moderate and high Reynolds numbers in which nonlinearity and complex vortex dynamics are important remain unclear.

The effects of shear-thinning fluids on fully developed turbulence in pipes were explored experimentally by Park et al. (1989), Pinho and Whitelaw (1990) and Escudier and Presti (1996). They found that compared to Newtonian fluids, shear-thinning fluids delay the transition to turbulence, reduce radial and tangential turbulent velocity fluctuations, and reduce the skin friction coefficient. More recently, a comprehensive set of direct numerical simulations of fully developed turbulent pipe flow using a power law fluid model and Herschel-Bulkley model (yield stress + shear thinning) were performed by Rudman et al. (2004). They argue, in agreement with the above cited experiments, that the dominant instabilities leading to wall-bounded turbulence have their origin very near the wall of a pipe or channel. They found that shear-thinning fluids reduce skin friction, tangential and wall normal velocity fluctuations, streamwise vorticity fluctuations, and Reynolds stresses in agreement with experimental findings. They also observed that the so-called ‘streak spacing’, a cross-stream length scale characterizing the spacing of quasi-periodic coherent structures found in wall-bounded turbulence

(Smith and Metzler, 1983), increases as the fluid becomes increasingly shear-thinning. Flow visualizations revealed that as shear-thinning was increased the flow became more intermittent in character, signifying that the flow was characterized by regions of quiescent laminar flow interspersed with fully turbulent regions. The authors conjecture that these relaminarization effects may be caused in part by the mixing of higher viscosity core fluid with wall fluid, thereby inhibiting the growth of near wall instabilities. These near wall instabilities, at least with respect to linear theory, have been recently explored by Nouar et al. (2007) for the flow of a shear-thinning Carreau fluid in channel flow. The authors looked at infinitesimal disturbances. They found that Carreau fluids may be able to delay the transition to turbulence in contrast to earlier investigations of linear stability in shear-thinning fluids. This difference is attributed to their choice of Reynolds number (based on the wall viscosity) and also to the inclusion of the effects of flow perturbations on the local viscosity, which was not taken into account in earlier work.

1.2 Objective

The great complexity of fully developed turbulence in pipes and channels, together with a need to understand the effects of non-Newtonian flows free of elasticity, leads to our present investigation. For this purpose, we focus here on the effects of solely shear-thinning fluids on the fundamental element of wall-bounded turbulence, the hairpin vortex. By focusing exclusively on shear-thinning fluids we avoid the complicating

effects associated with elasticity, namely the ability of viscoelastic fluids to enhance elongational viscosity (Lumley, 1969; Lumley, 1973). Moreover, by investigating the fully nonlinear evolution of hairpin vortices in fluids of increasingly greater shear-thinning capacity, we hope to simplify the more complex problem of understanding the effects of shear-thinning fluids on fully developed turbulence, as well as to gain more precise information on the mechanisms responsible for the apparent ability of such fluids to delay the transition to turbulence. We note that the evolution of a hairpin vortex in a shear flow, though not as complex as the evolution of fully developed turbulence, is still a flow in which fully nonlinear hydrodynamics modifies the local fluid viscosity in space and time. This is to be distinguished from the purely linear stability analyses cited previously. Recent work by Kim et al. (2008) and Kim and Sureshkumar (2013) illustrate the effectiveness of this approach. In their work, they explored the effects of a viscoelastic fluid (FENE-P model) on the evolution of a single hairpin vortex and showed that viscoelasticity strongly suppressed the growth of hairpins to the point where autogeneration was entirely suppressed in some cases, thereby eliminating the development of hairpin vortex packets. These are the only articles about hairpin in viscoelastic fluids we found. We are the first to investigate the effects of shear-thinning fluids on the evolution of hairpins.

1.3 Explanation for the Formation of a Hairpin

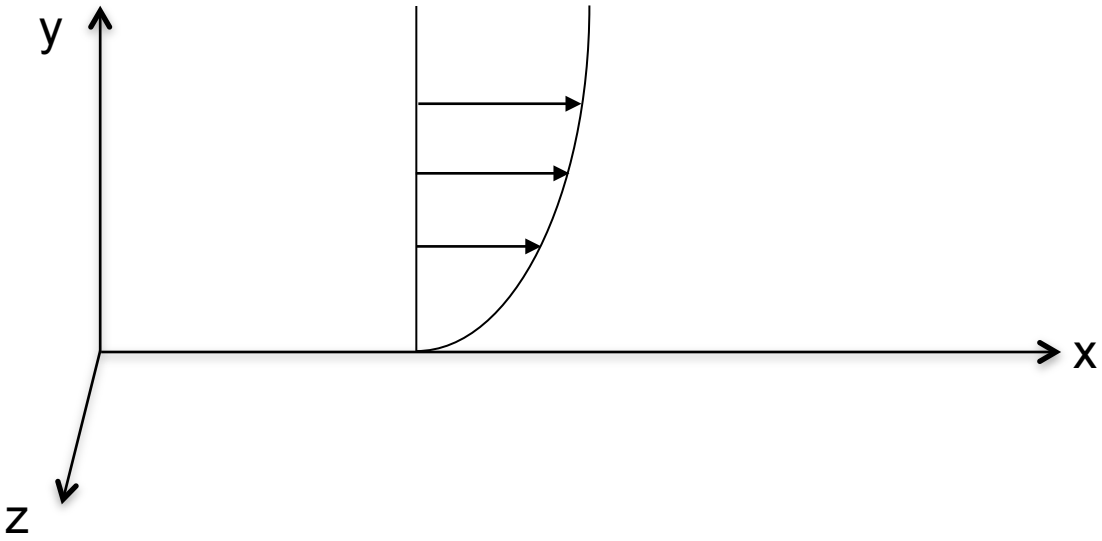

Figure 1.1: Instantaneous schematic representation of streamwise parabolic velocity profile

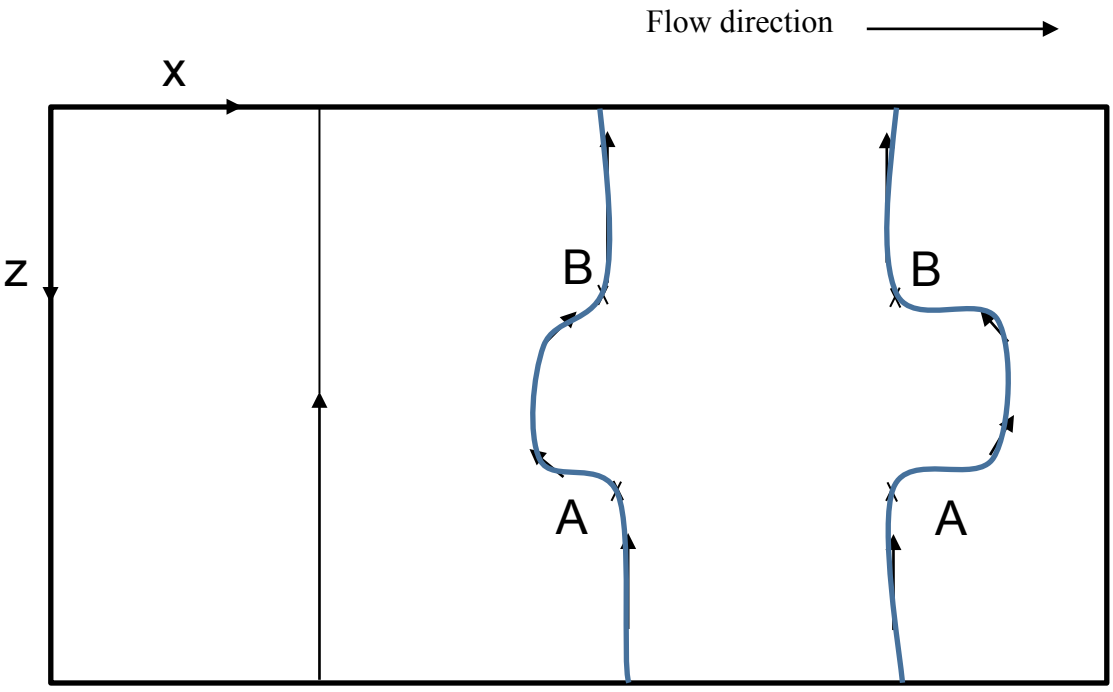

Figure 1.2: Vortex lines and two possible types of perturbation

Here we have a Newtonian flow with a parabolic velocity profile as shown in figure 1.1. The arrows point to the direction of the flow. Vortex lines are in x-z plane pointing towards the -z direction. The vorticity in the z direction Ω_z is given as:

$$\Omega_z = \left.\frac{\partial v}{\partial x}\right|_{y=0} - \left.\frac{\partial u}{\partial y}\right|_{y=0} \tag{1.1}$$

At $y = 0$, $u = v = w = 0$. Ω_z is at its maximum with $\Omega_z = -\left.\frac{\partial u}{\partial y}\right|_{y=0} \neq 0$

We are looking at a plane close to the wall. There is a slight perturbation in one of vortex lines as shown in figure 1.2. There are two kinds of equally likely perturbation in the forms of kinks as illustrated in figure 1.2. They are drawn with exaggeration here. Right thumb points to the direction of the arrows. The marked points are highlighted with tiny crosses in the following figures. For the first kind of perturbation illustrated at the left of figure 1.2, the vortex leg at point A presses the vortex leg at point B towards the wall, and vice versa. It will eventually dissipate when it interacts with the wall. The first kind of perturbation will not survive. For the second kind of perturbation illustrated on the right of figure 1.2, the vortex leg at point A lifts the vortex leg at point B, and vice versa, the so-called mutual induction according to the Biot-Savart law. A hairpin is formed. We assume viscosity is not important for a short period time, therefore we can treat the flow as an inviscid fluid. In this case, vortex lines are material lines. In another words, the vortices move with the fluid. t^* is the diffusion time scale which is also the time scale of dissipation due to viscosity. t is time scale at which the hairpin moves. υ is the kinematic viscosity. U_∞ is the centerline velocity.

$$t^* \sim \frac{D^2}{\upsilon} > t = \frac{D}{U_\infty} \tag{1.2}$$

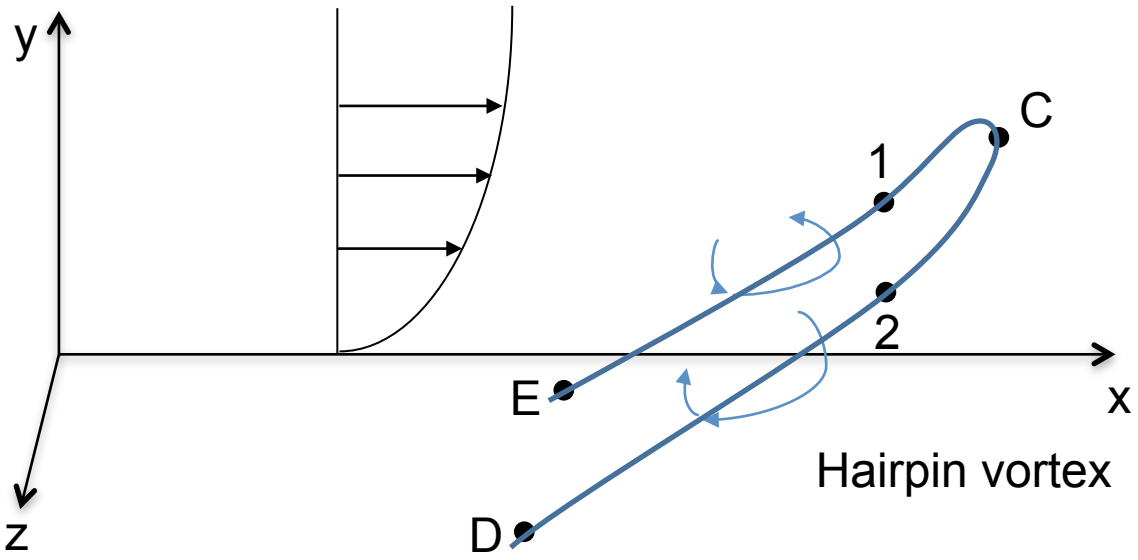

Figure 1.3: Hairpin vortex

A strong initial core will not diffuse quickly since inertial forces are larger than viscous forces. In figure 1.3, the vortex line at point C moves faster than the vortex lines at point E and point D, since they move at the speed as the velocity profile at the same elevation. Vorticiy is intensified due to vortex stretching. The head lifts up more rapidly than the legs. The lift-up is strongest at the narrow bridge which has the minimum spanwise separation. The momentum of inertia and the diameter of the vortex tube decrease. As a consequence, the vorticity is further intensified due to the conservation of angular momentum. The analogy will be that a figure skater spins faster on the ice when she pulls her arm closer to her body.

As illustrated in figure 1.3, point 1 is on the streamline of point 2 and the direction of the velocity on that streamline is upwards. As a consequence, Point 1 is lifted up. For the same reason, point 2 is also lifted up by point 1. There are disturbances behind the parent hairpin which generates secondary hairpins. The above explanation is qualitative, not quantitative. For example, it does not contain information regarding the minimal width of perturbation which is required to generate a hairpin. We assume what is true for one hairpin might be true for every hairpin.

2. PROBLEM FORMULATION AND NUMERICAL METHODS

2.1 Problem Formulation

We consider a fluid of constant density governed by the laws of momentum and mass conservation given by:

$$\frac{\partial u_i}{\partial t} + u_j \partial_j u_i = -\partial_i p + \partial_j T_{ji} + f_i \qquad (2.1)$$

$$\partial_i u_i = 0 \qquad (2.2)$$

where $u_j = (u_1, u_2, u_3) = (u, v, w)$ is the fluid velocity with components u, v and w in the x, y and z directions respectively, and t is time. The pressure divided by density is given by p, f_i is a body force, the viscous stress tensor divided by the density is given by $T_{ji} = 2\nu S_{ji}$, where $S_{ji} = (\partial_j u_i + \partial_i u_j)/2$ is the rate of strain tensor and ν is the kinematic viscosity.

Since we are focused on non-Newtonian fluids without elasticity, there are a fairly limited number of rheological models of this type available, including the Carreau, Ellis, Bingham plastic, Herschel-Bulkley, Casson, and the power law model (Chhabra and Richardson, 1999). In this dissertation, we have chosen the power-law model for two principal reasons: (1) The power law model, although it is the simplest of the models named above, applies to a very wide variety of flows, and (2) The phenomenon we investigate, namely the nonlinear evolution of hairpin vortices in a shear flow, is extremely complex even for a Newtonian fluid, so using a model more complex than the

simplest one which is the power law model creates an unnecessary degree of complexity. In the standard power law model (Tanner, 1988) used here, the kinematic viscosity which is a function of both space and time is given by:

$$\nu = K\dot{\gamma}^{n-1} = K\left(\sqrt{2S_{ji}S_{ji}}\right)^{n-1} \tag{2.3}$$

where $n > 0$ is the flow index, and K is the traditional fluid 'consistency' divided by density with units of $cm^2 \cdot s^{n-2}$. We note that when $n = 1$, the equations of motion reduce to that of a Newtonian fluid. Shear thinning behavior is obtained for $n < 1$, while the fluid is shear thickening when $n > 1$. In all our simulations, the fluid will be either Newtonian or shear thinning.

The equations of motion (2.1) and (2.2) together with the power law model given by (2.3) were solved using a pseudo-spectral code in a half-channel geometry in which the velocity field is expanded in Fourier modes in the horizontal $x - z$ plane and Chebyshev modes in the vertical y direction. The body force in (2.1) is chosen to act solely in the x direction, is constant in space and time so as to represent a constant driving pressure gradient, and is designated hereafter as f_x. The computational domain is illustrated in figure 2.1. The resolution which is the number of grid nodes was $128\times65\times128$ in the x, y and z directions respectively, and the corresponding domain lengths were $L_x = 4\pi D$, $L_y = D$, and $L_z = \pi D$, where D is the height of the half-channel. The domain extends from $y = -D$ at the bottom of the channel where no-slip boundary conditions $(u = w = v = 0)$ are enforced to $y = 0$ at the top, where shear-free conditions $(\partial u/\partial y = \partial w/\partial y = v = 0)$ are employed.

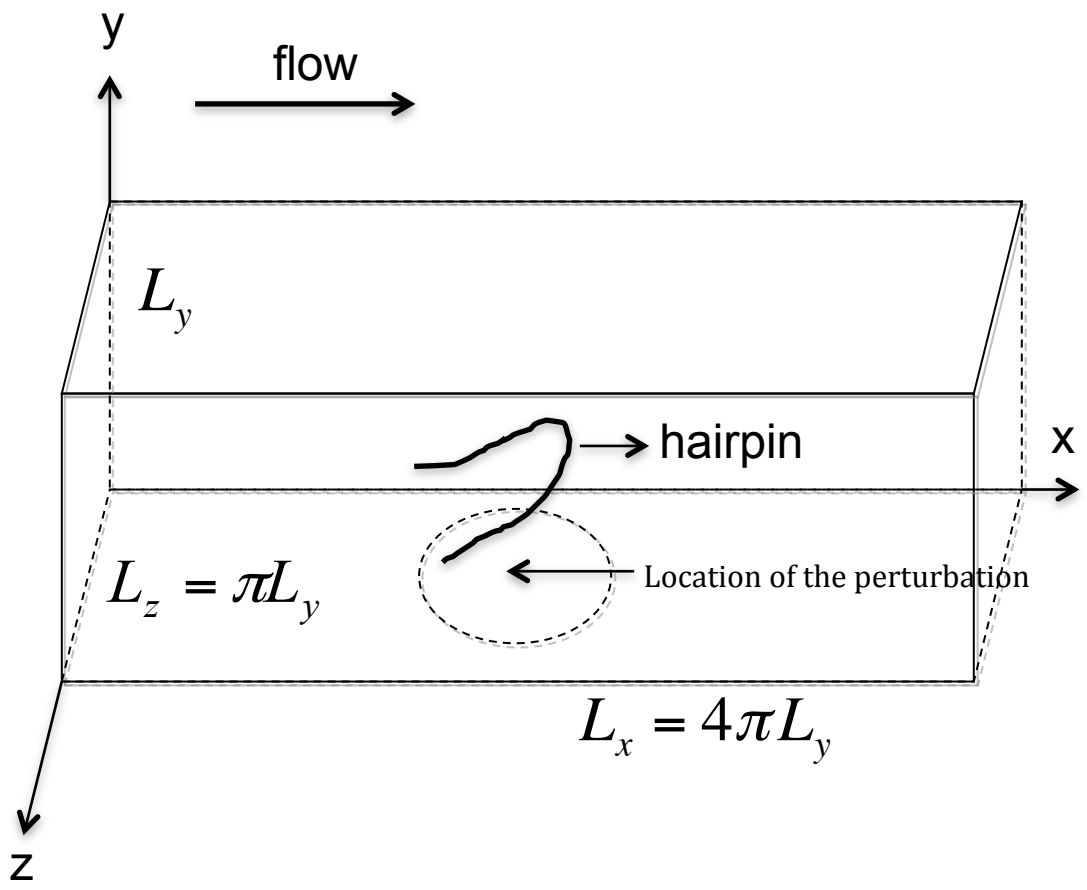

Figure 2.1: Schematic of the computational domain showing the body force perturbation used to create a hairpin vortex.

A 2 step process was used to generate a hairpin flow field. Firstly, a body force was added to a Newtonian flow. This Newtonian flow had initial velocities of 0 in all 3 directions. The body force acted in a Newtonian flow for 0.05 second. The center of the body force is at $2\pi D$ in the x direction, $-0.9D$ in the y direction and $0.5\pi D$ in the z direction. It is located near the wall and acts in the negative x direction. The force distribution has hyperbolic tangent profiles in all three directions. The amplitude decays

more rapidly in the y direction versus the other 2 directions. The data of the velocity field was printed out every 0.005 second. The data of the velocity field at 0.02 second was chosen.

Secondly, this data was added to another Newtonian flow and another simulation was performed. This Newtonian flow has the initial velocities as $(u, v, w) = (u_{th}(y), 0,0)$ and $Re = 5000$. The simulation lasted for 0.5 second. The data of the velocity field was printed out every 0.05 second. It was empirically determined that a mature hairpin was produced after 0.1 second and the velocity field at this time instant was chosen to initialize all subsequent simulations. The velocity field of the mature hairpin $\vec{V}_{hp} = \left(U_{hp}, V_{hp}, W_{hp}\right)$ is divergence free and satisfies the boundary conditions. If the same body force were to be used in all the simulations, the initial condition would not be identical. The same initial condition is used in all the simulations which cannot be performed experimentally in a laboratory.

In each case to be described below the initial condition was composed of an analytically determined laminar velocity profile $(u, v, w) = (u_{th}(y), 0,0)$ to which the hairpin flow field was added. The analytical solution for a steady laminar flow of a power law fluid in a half-channel driven by a constant pressure gradient f_x is given by:

$$u_{th}(y) = \frac{K}{f_x}\frac{n}{n+1}\left[\left(\frac{f_x}{K}D\right)^{\frac{1}{n}+1} - \left(-\frac{f_x}{K}y\right)^{\frac{1}{n}+1}\right] \qquad (2.4)$$

Here the pressure gradient is determined to precisely balance the wall shear associated with this analytically determined profile such that if the initial hairpin flow field eventually decays to zero, the flow will return to this state.

The initial condition for all runs is given explicitly by:

$$\left.\begin{aligned} \mathrm{u} &= \mathrm{u}_{\mathrm{th}}(y) + C_{hp}\left(U_{hp} - \left\langle U_{hp}\right\rangle\right) + C_{rand}\,u_{rand} \\ \mathrm{v} &= C_{hp}V_{hp} + C_{rand}\,v_{rand} \\ \mathrm{w} &= C_{hp}W_{hp} + C_{rand}\,w_{rand} \end{aligned}\right\} \qquad (2.5)$$

where $\langle U_{hp}\rangle = \frac{1}{L_x L_z}\int_0^{L_z}\int_0^{L_x} U_{hp}(x,y,z)\,dx\,dz$ is the horizontal average of the x component of the Newtonian flow which contained both a parabolic mean profile and a hairpin flow, and the symbol $\langle \ldots \rangle$ will be used subsequently to define instantaneous horizontal averaging. Here C_{hp} is a constant which sets the amplitude of the initial strength of the hairpin vortex, and C_{rand} is a constant used to vary the amplitude of a spatially random flow field given by $(u_{rand}, v_{rand}, w_{rand})$. The impulsive body force used to create the hairpin vortex was symmetric in the $x-z$ plane, and this symmetry was transferred to the hairpin vortex flow field. Thus the random flow field was introduced to break this initial symmetry, and was chosen to have a very low amplitude so as not to affect the spatial coherence of the hairpin. This breaking of symmetry allows the flow to develop in a more realistic manner. The initial strength of the hairpin produced in this way, characterized by its root-mean-square velocity (rms), was chosen to be approximately 2 to 4 percent of the initial maximum velocity in the channel, $u_{th}(0)$, and the rms of the random velocity field was about five percent of the rms velocity associated with the hairpin. It is important to note that the amplitude of the disturbance composed of both the hairpin vortex and the random velocity field is independent of 'n' and Reynolds number, and has horizontal zero mean. In addition,

while u_{th} changes from run to run, the absolute amplitude of the perturbation remains unchanged.

The main objective of this dissertation is to explore the effect of the Reynolds number and 'n' on the evolution of the hairpin vortex flow defined previously. That is, in each computer simulation series, we fix the Reynolds number, $Re = \frac{u_{th}(y=0:n,K)D}{\nu_{th}(n,K)}$ while varying 'n' where ν_{th} is the viscosity computed using $u_{th}(y)$ and (2.14) at the no-slip boundary. Note that this definition uses only quantities computed a priori. Another option is to define a Reynolds number using the volumetrically averaged initial viscosity associated with $u_{th}(y)$. However, for a variety of reasons delineated in detail in (Rudman et al., 2004; Nouar et al., 2007), the Reynolds number defined above is most appropriate for power law fluids. Most importantly, since instabilities in wall bounded turbulence are known to grow most rapidly near a no-slip wall, at least as far as linear stability theory is concerned (Rosenhead, 1963), this definition seems appropriate on physical grounds since it is based on the initial viscosity at the wall.

Simulations of hairpin vortex evolution were made for $Re = 4{\times}10^3, 6{\times}10^3, 8{\times}10^3$ and values of 'n' which range from 1.0 to 0.7. For the highest Reynolds number ($Re = 8{\times}10^3$), the grid resolution is $\Delta x{\sim}10l^+$ and $\Delta z{\sim}3l^+$ in the x and z directions respectively, where $l^+ = \nu_{th}/u^*$, $u^* = \sqrt{\tau/\rho}$ is the friction velocity, and τ is the shear stress at the no-slip boundary computed from $u_{th}(y)$ and the definition of the viscous stress tensor. Finally, since the power law model predicts an infinite viscosity at zero strain rate, it was necessary to use a 'cut-off' strain rate of 10^{-5} times the maximum

strain rate determined from $u_{th}(y)$ to preserve finite viscosity. A similar cutoff was used in (Rudman et al., 2004).

2.2 Numerical Methods

We rewrite the momentum equation as:

$$\frac{\partial u_i}{\partial t} = -\partial_i p - u_j \partial_j u_i + \partial_j T_{ji} + f_i \qquad (2.6)$$

We decompose the viscous term into two parts as shown below:

$$T_{ji} = 2\nu S_{ji} = 2\nu_0 S_{ji} + 2(\nu - \nu_0) S_{ji} \qquad (2.7)$$

$$\partial_j T_{ji} = 2\nu_0 \partial_j S_{ji} + \partial_j \left[2(\nu - \nu_0) S_{ji} \right] \qquad (2.8)$$

However, $2\nu_0 \partial_j S_{ji} = \nu_0 \partial_j \partial_j u_i = \nu_0 \nabla^2 u_i$

We then rewrite the momentum equation as:

$$\frac{\partial u_i}{\partial t} = -\partial_i p + \nu_0 \nabla^2 u_i + \partial_j \left[2(\nu - \nu_0) S_{ji} \right] - u_j \partial_j u_i + f_i \qquad (2.9)$$

In all our calculations, $\left[f_1 = f_x, f_2 = f_3 = 0 \right]$

ν_0 is the minimum viscosity or initial viscosity at the wall which is a constant. It is numerically difficult to solve $\partial_j T_{ji}$ directly using implicit method. The implicit Crank-Nicolson method is used for $\nu_0 \nabla^2 u_i$ while the explicit Adams-Bashforth method is used for $\partial_j \left[2(\nu - \nu_0) S_{ji} \right]$. While using an explicit method, we subtract ν_0 in order to avoid numerical instability.

In this dissertation, we refer to the numerical procedures developed in (Kim et al., 1987). By introducing $H_i = \partial_j \left[2(\nu - \nu_0) S_{ji} \right] - u_j \partial_j u_i + f_i$, the momentum equation can be rewritten as:

$$\frac{\partial u_i}{\partial t} = -\partial_i p + \nu_0 \nabla^2 u_i + H_i \tag{2.10}$$

$$\partial_i u_i = 0 \tag{2.2}$$

By reducing equations (2.10) and (2.2), a fourth-order equation for v and a second-order equation for the normal component of the vorticity are obtained as the following:

$$\frac{\partial}{\partial t} \nabla^2 \mathrm{v} = h_{\mathrm{v}} + \nu_0 \nabla^4 \mathrm{v} \tag{2.11}$$

$$\frac{\partial}{\partial t} g = h_{\mathrm{g}} + \nu_0 \nabla^2 \mathrm{g} \tag{2.12}$$

$$f + \frac{\partial \mathrm{v}}{\partial y} = 0 \tag{2.13}$$

where $f = \frac{\partial u}{\partial x} + \frac{\partial w}{\partial z}$, $g = \frac{\partial u}{\partial z} - \frac{\partial w}{\partial x}$

$$h_v = -\frac{\partial}{\partial y} \left(\frac{\partial H_1}{\partial x} + \frac{\partial H_3}{\partial z} \right) + \left(\frac{\partial^2}{\partial x^2} + \frac{\partial^2}{\partial z^2} \right) H_2$$

$$h_g = \frac{\partial H_1}{\partial z} - \frac{\partial H_3}{\partial x}$$

A spectral method is implemented in which the spatial derivatives of the velocity field is expanded with Fourier series in the streamwise and spanwise direction, Chebyshev polynomials in the normal direction. Equation (2.12) then becomes the following:

$$\left(1-\frac{\nu_0\Delta t}{2}\nabla^2\right)\mathrm{g}^{n+1}=\frac{\Delta t}{2}\left(3h_g^n-h_g^{n-1}\right)+\left(1+\frac{\nu_0\Delta t}{2}\nabla^2\right)\mathrm{g}^n$$

$$g\left(y=-L_y\right)=\left.\frac{\partial g}{\partial y}\right|_{y=0}=0 \qquad (2.14)$$

Equation (2.14) is transformed in the streamwise and spanwise directions with Fourier series and then each wavenumber is solved using the Chebyshev-tau method (Lanczos, 1956). The even and odd modes of the Chebyshev coefficients are decoupled and equation (2.14) becomes a tridiagonal system with one full row.

The fourth-order equation (2.11) can be solved efficiently after it was split into the two following second-order equations:

$$\left(1-\frac{\nu_0\Delta t}{2}\nabla^2\right)\phi^{n+1}=\frac{\Delta t}{2}\left(3h_{\mathrm{v}}^n-h_{\mathrm{v}}^{n-1}\right)+\left(1+\frac{\nu_0\Delta t}{2}\nabla^2\right)\phi^n$$

$$\nabla^2\mathrm{v}^{n+1}=\phi^{n+1}$$

$$\mathrm{v}^{n+1}\left(y=-L_y\right)=\frac{\partial \mathrm{v}^{n+1}}{\partial y}\left(y=-L_y\right)=\mathrm{v}^{n+1}\left(y=0\right)=\frac{\partial^2 \mathrm{v}^{n+1}}{\partial y^2}\left(y=0\right)=0 \qquad (2.15)$$

We can rewrite the continuity equation as:

$$\frac{\partial u}{\partial x}+\frac{\partial v}{\partial y}+\frac{\partial w}{\partial z}=0$$

We then take the derivative of the continuity equation with respect to y:

$$\frac{\partial}{\partial x}\left(\frac{\partial u}{\partial y}\right)+\frac{\partial^2 v}{\partial y^2}+\frac{\partial}{\partial z}\left(\frac{\partial w}{\partial y}\right)=0$$

$$\left.\frac{\partial^2 v}{\partial y^2}\right|_{y=0}=0 \text{ since } \left.\frac{\partial u}{\partial y}\right|_{y=0}=\left.\frac{\partial w}{\partial y}\right|_{y=0}=0$$

The Chebyshev-tau method is used to solve this coupled system. The four boundary conditions are satisfied as listed below. Let:

$$v^{n+1} = v_p^{n+1} + c_1 v_1^{n+1} + c_2 v_2^{n+1}, \tag{2.16}$$

where the particular solution v_p^{n+1} as well as the two homogeneous solutions v_1^{n+1} and v_2^{n+1} satisfy

$$\left(1 - \frac{\nu_0 \Delta t}{2} \nabla^2\right) \phi_p^{n+1} = \frac{\Delta t}{2} \left(3 h_v^n - h_v^{n-1}\right) + \left(1 + \frac{\nu_0 \Delta t}{2} \nabla^2\right) \phi^n$$

$$\phi_p^{n+1}(\pm 1) = 0$$

$$\nabla^2 v_p^{n+1} = \phi_p^{n+1},\ v_p^{n+1}(\pm 1) = 0 \tag{2.17}$$

$$\left(1 - \frac{\nu_0 \Delta t}{2} \nabla^2\right) \phi_1^{n+1} = 0$$

$$\phi_1^{n+1}(1) = 0, \phi_1^{n+1}(-1) = 1$$

$$\nabla^2 v_1^{n+1} = \phi_1^{n+1},\ v_1^{n+1}(\pm 1) = 0 \tag{2.18}$$

$$\left(1 - \frac{\nu_0 \Delta t}{2} \nabla^2\right) \phi_2^{n+1} = 0$$

$$\phi_2^{n+1}(1) = 1, \phi_2^{n+1}(-1) = 0$$

$$\nabla^2 v_2^{n+1} = \phi_2^{n+1}, v_2^{n+1}(\pm 1) = 0 \tag{2.19}$$

Equations (2.17) (2.18) (2.19) are transformed using Fourier series in the streamwishe and spanwise directions. They are then solved simultaneously by removing the same

banded matrix with three different right-hand sides. The constants c_1 and c_2 are chosen to satisfy the following criteria:

$$\frac{\partial \mathrm{v}^{n+1}}{\partial y}\left(y=-L_y\right)=\frac{\partial^2 \mathrm{v}^{n+1}}{\partial y^2}\left(y=0\right)=0 \qquad (2.20)$$

After the normal velocity and vorticity are calculated, using equation (2.5) and the definitions of f and g, the streamwise velocity u and the spanwise velocity w can then be calculated. Time advancement does not require the calculation of pressure. By computing pressure, turbulence statistics involving pressure can be obtained. We can compute the pressure from the normal momentum equation. The wall pressure values are determined from the combination of streamwise and spanwise momentum equations which are the governing equations of f. We can also compute pressure from the equation for f. The pressure corresponding to the zero wavenumbers $\left(k_x=k_z=0\right)$ is determined from the normal momentum equation. The two methods produce the same results for the present numerical method which implies the pressure satisfies both the Neumann and Dirichlet boundary conditions (Moin and Kim, 1980). Some other spectral codes do not preserve this consistency requirement.

In order to preserve the conservation of mass, energy and circulation numerically, the nonlinear terms in equation (2.1) are calculated in the rotational form (Moin and Kim, 1982). Additionally, prior to transforming into the physical space, the number of collocation points is expanded by a factor of 1.5 to avoid the aliasing errors due to calculating the nonlinear terms pseudo-spectrally.

2.3 Simulation Parameters

Table 2.1 List of all the runs

Run	Re	n	hpe	crand	DT	time steps	real time (s)
1	4000	1	5	0.001	0.000025	160000	4
2		0.9					
3		0.8					
4		0.7					
5	6000	1	0.1	0.001	0.000025	400000	10
6		0.7					
7		1	1				
8		0.7					
9		1	5				
10		0.9				200000	5
11		0.8					
12		0.7					
13		1	10				
14		0.9					
15		0.7			0.0000125	800000	10
16	8000	1	5	0.001	0.000025	200000	5
17		0.9					
18		0.8					
19		0.7					

3. RESULTS

3.1 The Derivation of the Kinetic Equation for a Non-Newtonian Flow during Transient

It is not the primary purpose of this dissertation to elucidate the detailed evolution and topological structure of an individual hairpin in a shear flow, which has been investigated in detail by others for a Newtonian fluid (Adrian, 2007; Zhou et al., 1999). Instead we want to obtain a global understanding of the evolution of the flow, which can be obtained by calculating the volumetric average of the kinetic energy of the fluctuations.

In our calculations, we simulate transients that are not statistically steady. In order to derive the kinetic energy equation, we start with the momentum equation:

$$\frac{\partial u_i}{\partial t} + u_j \partial_j u_i = -\partial_i p + \frac{\partial}{\partial x_j}\tau_{ij} \tag{3.1}$$

$$u_i = \langle u_i \rangle + u_i'$$

$$\langle u_i \rangle = \langle u_i \rangle + \langle u_i' \rangle$$

$$\langle u_i' \rangle = 0$$

u_i is the total velocity. The bracket designates the horizontal average defined by $\langle \varphi \rangle = \frac{1}{L_x L_z}\int_0^{L_z}\int_0^{L_x} \varphi dx\, dz$. $\langle u_i \rangle$ is the horizontal average of the total velocity. u_i' is the

fluctuating velocity field. The overbar designates the volumetric average defined by $\bar{\phi} = \frac{1}{L_x L_y L_z}\int_0^{L_z}\int_{-L_y}^{0}\int_0^{L_x}\phi(x,y,z,t)dx\,dy\,dz$

We now list the boundary conditions at the shear free top boundary and the no-slip bottom boundary:

Top $x_2 = 0$: $u_2 = 0$, $\frac{\partial u_1}{\partial x_2} = \frac{\partial u_3}{\partial x_2} = 0$, $\frac{\partial^2 u_2}{\partial x_2^2} = 0$

Bottom $x_2 = -L$: $u_1 = u_2 = u_3 = 0$

Top: $\langle u_2 \rangle = 0$, $\frac{\partial \langle u_1 \rangle}{\partial x_2} = \frac{\partial \langle u_3 \rangle}{\partial x_2} = 0$

Bottom: $\langle u_1 \rangle = \langle u_2 \rangle = \langle u_3 \rangle = 0$

Top: $u_2 = 0$, $\frac{\partial u_1'}{\partial x_2} = \frac{\partial u_3'}{\partial x_2} = 0$, $u_1' \neq 0$, $u_3' \neq 0$

Bottom: $u_1' = u_2' = u_3' = 0$, $\frac{\partial u_2'}{\partial x_2} = 0$ due to mass conservation, $\frac{\partial u_2'}{\partial x_1} \neq 0$, $\frac{\partial u_2'}{\partial x_3} \neq 0$

Unsteady term

$$\overline{u_i' \frac{\partial\left(\langle u_i \rangle + u_i'\right)}{\partial t}} = \overline{u_i' \frac{\partial u_i'}{\partial t}} + \overline{u_i' \frac{\partial \langle u_i \rangle}{\partial t}}$$

$$\overline{u_i' \frac{\partial \langle u_i \rangle}{\partial t}} = \frac{1}{L_x L_y L_z}\int u_i' \frac{\partial \langle u_i \rangle}{\partial t} dxdydz$$

$$= \frac{1}{L_x L_y L_z}\int\left(\int u_i' dx\,dz\right)\frac{\partial \langle u_i \rangle}{\partial t} dy = \frac{1}{L_x L_y L_z}\int \overline{u_i'} \frac{\partial \langle u_i \rangle}{\partial t} dy = 0$$

since $\overline{u_i'} = 0$, $\langle u_i \rangle$ is a function of y

$$\overline{u_i' \frac{\partial\left(\left\langle u_i \right\rangle + u_i'\right)}{\partial t}} = \overline{u_i' \frac{\partial u_i'}{\partial t}} = \frac{\partial k}{\partial t}$$

$k = \frac{1}{2}\overline{u_i' u_i'}$ represents the kinetic energy of the fluctuations

Convective term

$$\overline{u_i'\left(\left\langle u_j \right\rangle + u_j'\right)\partial_j\left(\left\langle u_i \right\rangle + u_i'\right)} = \overline{u_i'\left\langle u_j \right\rangle \partial_j \left\langle u_i \right\rangle} + \overline{u_i'\left\langle u_j \right\rangle \partial_j u_i'} + \overline{u_i' u_j' \partial_j \left\langle u_i \right\rangle} + \overline{u_i' u_j' \partial_j u_i'}$$

$$= \overline{u_i'\left\langle u_j \right\rangle \partial_j u_i'} + \overline{u_i' u_j' \partial_j \left\langle u_i \right\rangle} + \overline{u_i' u_j' \partial_j u_i'}$$

$\overline{u_i'\left\langle u_j \right\rangle \partial_j \left\langle u_i \right\rangle} = 0$ since $\overline{u_i'} = 0$

$$\partial_j\left(u_i' u_i' u_j'\right) = u_i' u_j' \partial_j u_i' + u_i' \partial_j\left(u_i' u_j'\right)$$

$$u_i' \partial_j\left(u_i' u_j'\right) = u_i' u_i' \partial_j u_j' + u_i' u_j' \partial_j u_i' = u_i' u_j' \partial_j u_i'$$

$$\partial_j\left(u_i' u_i' u_j'\right) = 2 u_i' u_j' \partial_j u_i'$$

$$\overline{u_i' u_j' \partial_j u_i'} = \overline{\partial_j\left(\frac{u_i' u_i'}{2} u_j'\right)}$$

$$\overline{u_i'\left(\left\langle u_j \right\rangle + u_j'\right)\partial_j\left(\left\langle u_i \right\rangle + u_i'\right)} = \overline{u_i'\left\langle u_j \right\rangle \partial_j u_i'} + \overline{u_i' u_j' \partial_j \left\langle u_i \right\rangle} + \overline{\partial_j\left(\frac{u_i' u_i'}{2} u_j'\right)}$$

$\left\langle u_1 \right\rangle \neq 0$, $\left\langle u_2 \right\rangle = \left\langle u_3 \right\rangle = 0$

$$\overline{u_i'\left\langle u_j \right\rangle \partial_j u'} = \overline{\left\langle u_1 \right\rangle u_i' \partial_1 u'} = \overline{\left\langle u_1 \right\rangle \partial_1\left(\frac{u_i' u_i'}{2}\right)} = \frac{1}{L_y}\int_y \left\langle u_1 \right\rangle \left\langle \partial_1\left(\frac{u_i' u_i'}{2}\right)\right\rangle dy$$

$$\left\langle \partial_1\left(\frac{u_i' u_i'}{2}\right)\right\rangle = 0$$

$$\overline{\partial_j\left(\frac{u_i'u_i'}{2}u_j'\right)}=0$$

$$f=\partial_j\left(\frac{u_i'u_i'}{2}u_j'\right)$$

$\int_0^{L_1}\frac{\partial f}{\partial x_1}dx_1=f\left(x_1=L_1,x_2,x_3\right)-f\left(0,x_2,x_3\right)=0$ due to periodicity in the x directions. The same is true for the z direction.

$\int_{-L}^{0}\frac{\partial\left(\frac{u_i'u_i'}{2}u_2\right)}{\partial x_2}dx_2=\frac{u_i'u_i'}{2}u_2'\Big|_0-\frac{u_i'u_i'}{2}u_2'\Big|_{-L}=0$ due to the boundary condition in the y direction.

$$\overline{u_i'\left(\left\langle u_j\right\rangle+u_j'\right)\partial_j\left(\left\langle u_i\right\rangle+u_i'\right)}=\overline{u_i'u_j'\partial_j\left\langle u_i\right\rangle}=\overline{u_1'u_2'\partial_2\left\langle u_1\right\rangle}=\overline{u_1'u_2'}\frac{\partial\left\langle u_1\right\rangle}{\partial x_2}$$

The terms representing the transport of kinetic energy including $\overline{u_i'\left\langle u_j\right\rangle\partial_j u_i'}$ and $\overline{u_i'u_j'\partial_j u_i'}$ are identically zero.

$P_1=\overline{u_1'u_2'}\frac{\partial\left\langle u_1\right\rangle}{\partial x_2}$ represents the production of turbulence due to shear

Pressure term

$$\overline{u_i'\partial_i\left(\left\langle p\right\rangle+p'\right)}=\overline{u_i'\partial_i p'}+\overline{u_i'\partial_i\left\langle p\right\rangle}$$

$\left\langle u_i'\partial_i\left\langle p\right\rangle\right\rangle=0$ since $\overline{u_i'}=0$

$$\partial_i\left(u_i'p'\right)=u_i'\partial_i p'+p'\partial_i u_i'=u_i'\partial_i p'$$

$\left\langle u_i' \partial_i \left(\left\langle p \right\rangle + p' \right) \right\rangle = \left\langle \partial_i \left(u_i' p' \right) \right\rangle = 0$ since p' is periodic and $u_2' = 0$ at both boundaries.

Viscous term

$$\mathrm{v} = u_i' \partial_j \tau_{ji}$$

$$\tau_{ji} = 2\nu S_{ji}$$

$$S_{ji} = \left\langle S_{ji} \right\rangle + \beta_{ji}$$

$$\mathrm{v} = u_i' \partial_j \left(2\nu S_{ji} \right) = u_i' \partial_j \left(2\nu \overline{S_{ji}} \right) + u_i' \partial_j \left(2\nu \beta_{ji} \right) = \mathrm{v}_2 + \mathrm{v}_1$$

$$\mathrm{v}_1 = u_i' \partial_j \left(2\nu \beta_{ji} \right)$$

$$\partial_j \left(2\nu u_i' \beta_{ji} \right) = u_i' \partial_j \left(2\nu \beta_{ji} \right) + 2\nu \beta_{ji} \partial_j u_i'$$

$$\partial_j u_i' = \beta_{ji} + \Omega_{ji}'$$

$$\mathrm{v}_1 = \partial_j \left(2\nu u_i' \beta_{ji} \right) - 2\nu \beta_{ji} \beta_{ji}$$

$$\mathrm{v}_2 = u_i \partial_j \left(2\nu \left\langle S_{ji} \right\rangle \right)$$

$$\partial_j \left(2\nu u_i' \left\langle S_{ji} \right\rangle \right) = u_i' \partial_j \left(2\nu \left\langle S_{ji} \right\rangle \right) + 2\nu \left\langle S_{ji} \right\rangle \partial_j u_i'$$

$$\mathrm{v}_2 = \partial_j \left(2\nu u_i' \left\langle S_{ji} \right\rangle \right) - 2\nu \left\langle S_{ji} \right\rangle \beta_{ji}$$

$$\overline{\partial_j \left(2\nu u_i' \beta_{ji} \right)} = \overline{\partial_1 \left(2\nu u_i' \beta_{1i} \right)} + \overline{\partial_2 \left(2\nu u_i' \beta_{2i} \right)} + \overline{\partial_3 \left(2\nu u_i' \beta_{3i} \right)}$$

$\overline{\partial_1 \left(2\nu u_i' \beta_{1i} \right)} = \overline{\partial_3 \left(2\nu u_i' \beta_{3i} \right)} = 0$ due to periodicity

$$\overline{\partial_2 \left(2\nu u_i' \beta_{2i} \right)} = \int \frac{\partial}{\partial x_2} \left(2\nu \overline{u_1' \beta_{21}} \right) dx_2 + \int \frac{\partial}{\partial x_2} \left(2\nu \overline{u_2' \beta_{22}} \right) dx_2 + \int \frac{\partial}{\partial x_2} \left(2\nu \overline{u_3' \beta_{23}} \right) dx_2$$

$\int \frac{\partial}{\partial x_2}\left(2\overline{\nu u_2' \beta_{22}}\right) dx_2 = 0$ since $u_2' = 0$ at the top and the bottom of the domain

$\beta_{ji} = \frac{1}{2}\left(\frac{\partial u_j'}{\partial x_i} + \frac{\partial u_i'}{\partial x_j}\right)$ represents the fluctuating part of the symmetric part of the velocity gradient tensor

$\beta_{21} = \frac{1}{2}\left(\frac{\partial u_2'}{\partial x_1} + \frac{\partial u_1'}{\partial x_2}\right)$ since $\beta_{12} = 0$ at the top, $u_2' = 0$, $\frac{\partial u_1'}{\partial x_2} = 0$ shear free

$\beta_{23} = \frac{1}{2}\left(\frac{\partial u_2'}{\partial x_3} + \frac{\partial u_3'}{\partial x_2}\right)$ since $\beta_{23} = 0$ at the top, $u_2' = 0$, $\frac{\partial u_3'}{\partial x_2} = 0$ shear free

$\int \frac{\partial}{\partial x_2}\left(2\langle \nu u_1' \beta_{21} \rangle\right) dx_2 = 0$ since $\beta_{21} = 0$ at top and $u_1' = 0$ on bottom

$\int \frac{\partial}{\partial x_2}\left(2\langle \nu u_3' \beta_{23} \rangle\right) dx_2 = 0$

$\overline{\mathrm{v}_1} = -\overline{2\nu \beta_{ji} \beta_{ji}}$

$\gamma = -\overline{2\nu \beta_{ji} \beta_{ji}}$ represents the dissipation.

$\langle S_{12} \rangle = \frac{1}{2}\frac{\partial \langle u_1 \rangle}{\partial x_2} = \langle S_{21} \rangle$

$\partial_j\left(2\nu u_i' \overline{S_{ji}}\right) = \partial_1\left(2\nu u_2' \overline{S_{12}}\right) + \partial_2\left(2\nu u_1' \overline{S_{21}}\right) = \partial_1\left(\nu u_2' \frac{\partial U_1}{\partial x_2}\right) + \partial_2\left(\nu u_1' \frac{\partial U_1}{\partial x_2}\right)$

$\overline{\mathrm{v}_2} = -\overline{2\nu \beta_{ji} \langle S_{ji} \rangle}$

$\beta_{ji}\langle S_{ji} \rangle = \beta_{12}\langle S_{12} \rangle + \beta_{21}\langle S_{21} \rangle = 2\beta_{12}\langle S_{12} \rangle = \beta_{12}\frac{\partial \langle u_1 \rangle}{\partial x_2}$

$\overline{\nu_2} = -2\overline{\nu\beta_{12}\frac{\partial\langle u_1\rangle}{\partial x_2}}$

$P_2 = -2\overline{\nu\beta_{12}\frac{\partial\langle u_1\rangle}{\partial x_2}}$ presents the production of turbulence due to non-Newtonian effects.

The evolution equation for k is therefore given by:

$$\frac{\partial k}{\partial t} = P_1 + P_2 - \gamma = -\overline{u_1' u_2'}\frac{\partial\langle u_1\rangle}{\partial x_2} - 2\overline{\nu\beta_{12}\frac{\partial\langle u_1\rangle}{\partial x_2}} - 2\overline{\nu\beta_{ji}\beta_{ji}} \qquad (3.2)$$

3.2 Effects of Reynolds Number and Power Law Index on the Evolution of a Hairpin Vortex

An overall view of the evolution of a hairpin vortex in a shear-thinning fluid can be obtained by observing the temporal evolution of the kinetic energy k of the flow. This is shown in figure 3.1 (Zhen et al., 2013) for a consistency $K = 10^{-2} cm^2 \cdot s^{n-2}$, which corresponds to the kinematic viscosity of water at 20℃ for $n = 1$. Results are shown for Reynolds numbers ranging from 4000 to 8000. For comparison, linear stability theory (Orszag, 1971) shows that the critical Reynolds number for plane (2-walled) channel flow is $Re = 5772$. We note of course that k is the same at $t = 0$ in all cases as a result of our choice of initial conditions described above. For each Reynolds number it is seen that the kinetic energy of the disturbance initially decreases, with the possible exception of $Re = 8{\times}10^3$ for $n = 1$, before rebounding, peaking, and subsequently decreasing. The effect of decreasing 'n' (increased shear thinning) is clearly to delay the appearance of the peak in the kinetic energy. For example, for $Re = 4{\times}10^3$ the maximum kinetic

energy for $n = 1$ occurs at $\sim 0.9s$ but for $n = 0.7$ the peak is significantly delayed to $\sim 1.6s$. Moreover, as 'n' decreases for each Reynolds number, the magnitude of the maximum value of k is significantly decreased, with the decrease typically one order of magnitude or more for the $n = 1$ case compared to that for $n = 0.7$. In each case, with the possible exception of $Re = 8{\times}10^3$ for $n = 1$, the rate of change of the kinetic energy, dk/dt, is negative at early times and its absolute value is clearly seen to increase with decreasing 'n', indicating that the effect of increased shear thinning is to accelerate the initial decrease in kinetic energy of the hairpin vortex. Finally, for any given value of 'n', as the Reynolds number increases, the peak in the kinetic energy appears earlier in time.

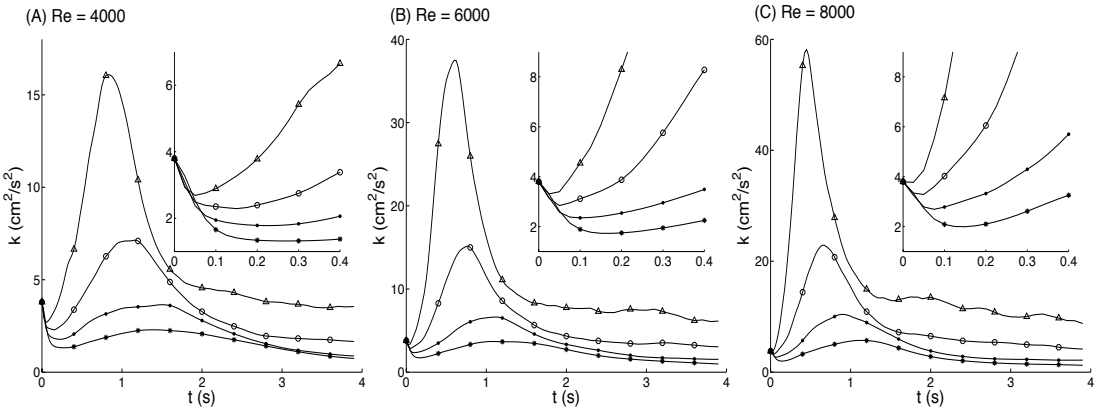

Figure 3.1. Kinetic energy $k(cm/s)^2$ versus time t (seconds) of channel flow perturbed by a hairpin vortex for three Reynolds numbers. Symbols represent the power law index n: $\triangle$ ($n = 1$, Newtonian), $\bigcirc$ ($n = 0.9$), $\cdot$ ($n = 0.8$), $*$ ($n = 0.7$). Reprint with permission from (Zhen et al., 2013).

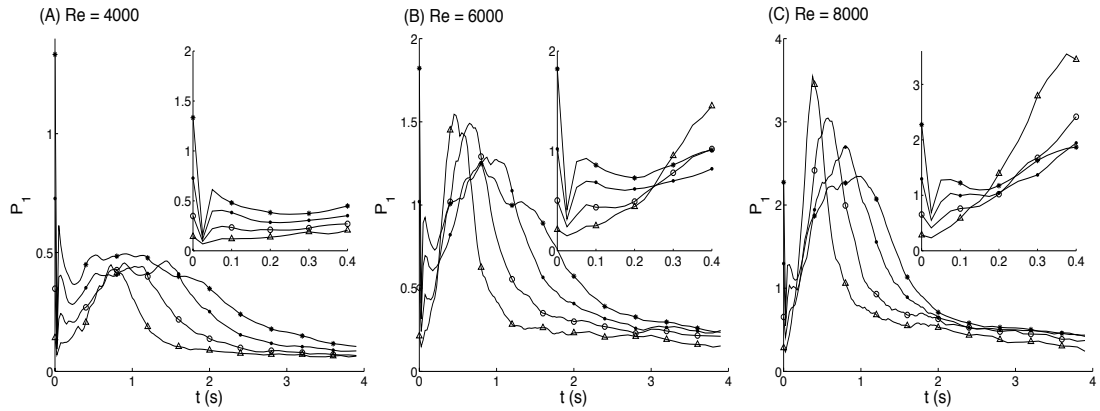

Figure 3.2. Production of kinetic energy P_1 made nondimensional by $(u^*)^4/\nu_{th}$ versus time t (seconds) for channel flow perturbed by a hairpin vortex for three Reynolds numbers. Symbols are identical to those in Figure 3.1. Reprint with permission from (Zhen et al., 2013).

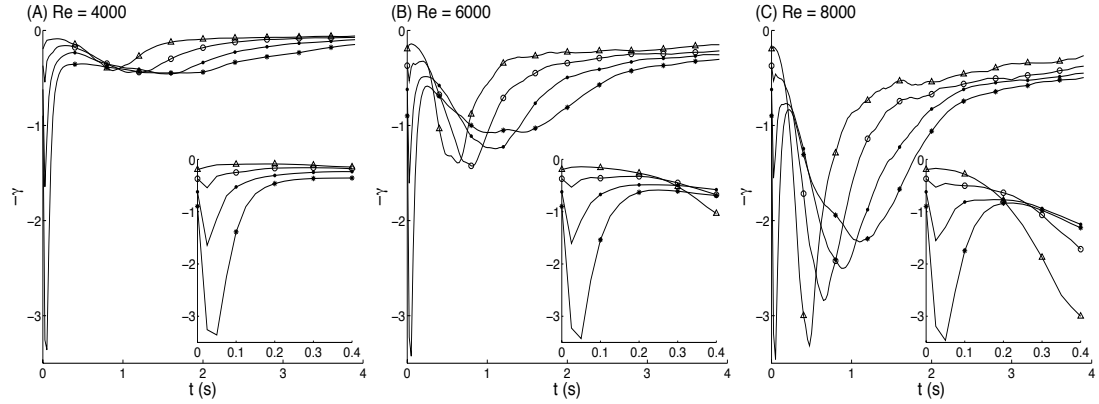

Figure 3.3. Dissipation of kinetic energy $-\gamma$ made nondimensional by $(u^*)^4/\nu_{th}$ versus time t (seconds) for a channel flow perturbed by a hairpin vortex for three Reynolds numbers. Symbols are identical to those in Figure 3.1. Reprint with permission from (Zhen et al., 2013).

We have found in all cases that the term P_2, which represents production of kinetic energy via non-Newtonian effects, is negligibly small (typically less than one percent of P_1) and will not be presented here. Further insight into these dynamics can be gained by studying the evolution of the production, P_1, and the dissipation, γ, in figures 3.2 and 3.3 (Zhen et al., 2013). In these figures, in order to insure a proper relative comparison of these terms, the quantities of interest are made non-dimensional using $(u^*)^4/\nu_{th}$, an estimate of the production and dissipation in each case. The production shown in figure 3.2 is seen to decrease from its initial value at very early times in all cases. However, as 'n' decreases, the initial time rate of change of the production becomes increasingly negative, indicating that shear thinning has a strong effect on the production of kinetic energy of the hairpin. Subsequently, the production is found to peak in all cases before decaying to levels which appear to be nearly steady for times greater than about 3 seconds. Interestingly, for $n < 1$, the production appears to exhibit two peaks, one at early times ($t{\sim}0.5s$) and a broader peak appearing later. The temporal evolution of the negative of the dissipation, $-\gamma$, is shown in figure 3.3. $-\gamma$ is plotted here since dissipation serves as a sink of the kinetic energy. The effect of shear thinning on dissipation is evident at $t = 0$ where for the Newtonian case, $d\gamma/dt$ is slightly negative whereas it becomes increasingly positive as n decreases. This indicates that the effect of shear thinning on the hairpin vortex is to immediately increase the rate at which it is being dissipated by viscous action. In the shear thinning cases a peak in the dissipation occurs very early in time ($t < 0.1s$), the magnitude of this peak being at least one order of magnitude larger for $n = 0.7$ compared to the Newtonian case near $t = 0$. Moreover,

for $n < 1$, the rapid increase in dissipation is followed by a nearly equally rapid decrease, followed again by an increase until a near steady state is reached at around $t{\sim}3s$.

The effect of a shear thinning fluid on the evolution of the production, and especially the rate of viscous dissipation, is particularly striking. It is therefore of some interest to see how the effects of shear thinning are manifested in the structure of the flow. For this purpose, we use the parameter λ_2, an eigenvalue of the sum of the squares of the rate of strain tensor and the rotation tensor, which has been shown (Jeong and Hussain, 1995) to be effective in identifying vortex cores. In figure 3.4, isosurfaces of λ_2 are shown at four time instants for $Re = 4{\times}10^3$. As specified by the initial conditions, the hairpin vortex is seen to be identical at $t = 0s$ for all values of 'n', and has the standard shape associated with such a vortex: two elongated 'legs' and an elevated 'head'. At $t = 0.05s$, which corresponds approximately to the time at which the dissipation is a maximum in the $n < 1$ cases, it appears that the hairpin vortex remains relatively intact in the Newtonian case, but as 'n' decreases the vortex is seen to progressively lose coherence, and appears to break up into smaller scale structures. In particular, for $n = 0.7$ and $t = 0.05$, the basic structure of the initial vortex becomes difficult to discern. At $t = 0.775s$ the initial hairpin evolves into a complex system of vortices in all cases, which upon closer examination not shown here, resembles a turbulent spot (Strand and Goldstein, 2011). However, as 'n' decreases, the strength of the vortices is seen to decrease. Finally at $t = 3.5s$, the elongated, rather robust vortex structures in the Newtonian case contrast with the weaker structures for the $\mathrm{n} = 0.7$ case.

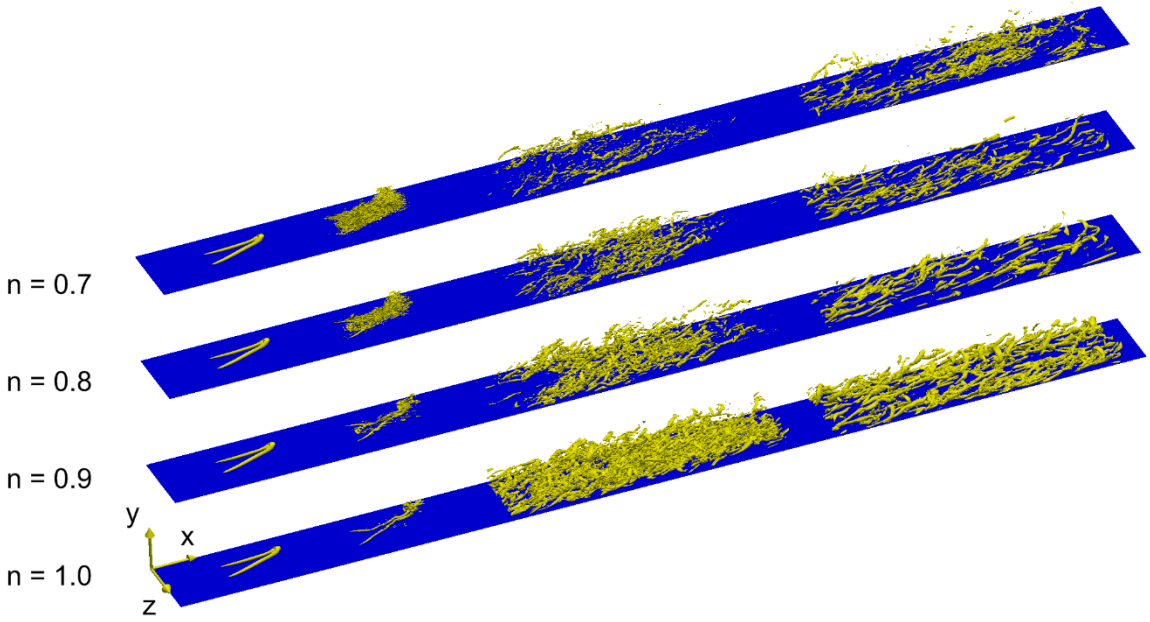

Figure 3.4. Three dimensional visualization of the evolution of λ_2 for a hairpin vortex in a channel flow for a Reynolds number of 4000. For each value of 'n', the times are $t = 0.0s$, $0.05s$, $0.775s$, and $3.5s$, with corresponding λ_2 levels of -10000, -4000, -2000, and -300. The mean flow is in the positive x direction. Reprint with permission from (Zhen et al., 2013).

Asymmetry is observed in all four cases in figure 3.4 (Zhen et al., 2013). Possible causes include the randomness of the calculation, the non-linear term in the Navier-Stokes equation, the added random noise and Gibbs oscillation, etc. It will take long time for round-off error to cause asymmetry.

These visualizations appear to be in good agreement with the quantitative results shown in figures 3.1-3.3 and suggest that the primary effect of shear thinning is to delay the transition of the initial perturbed laminar flow to a turbulent state. In particular, the

observed breakdown of the hairpin vortex into smaller scales occurs roughly at a time of maximal dissipation. This is in agreement with the fact that the dissipation, which is determined from the sum of the squares of velocity gradients, is disproportionately due to the smallest flow structures. This is demonstrated via the relation between the Fourier spectral density of the dissipation $D(k)$ and that of the velocity field, $E(k)$, given by $D(k) \propto k^2 E(k)$ where $k = 2\pi/\lambda$ is the wavenumber of an 'eddy' and λ is its wavelength (Batchelor, 1953; Tennekes and Lumley, 1972; Hinze, 1975). Apparently it is this rapid initial breakdown of the hairpin vortex in a shear thinning fluid that leads to the delay in the transition of the flow to a turbulent state. Dissipation is related to velocity gradient. Smaller structure leads to higher gradients which lead to dissipation.

3.3 The Effect of Hairpin Amplitude on the Evolution of the Flow

For Re = 6000, we choose hpe = 0.1, 1, 5 and 10, n = 1.0, 0.7 and we run the simulation for 10s in each case. We would like to see whether self-sustained turbulence can be achieved at 10 seconds. When hpe = 0.1, it looks like the perturbation in both cases dies out and the parabolic profile is restored after 2 seconds. When hpe = 10, in order to run the case where n = 0.7, the time step had to be cut in half versus the time step used in the cases where n = 1.0.

We present dimensional plots here.

For n = 1.0, for hpe = 1, 5 and 10, the maximum value of energy decreases as hpe increases as shown in figure 3.5. The maximum appears earlier in time as hpe increases.

In figure 3.6, the case where hpe = 5 has the highest value of production. In figure 3.7, the case where hpe = 10 has the highest value of dissipation. For hpe = 0.1, the values of energy, production and dissipation remain relatively flat and close to 0.

For n = 0.7, for hpe = 1, 5 and 10, the maximum value of energy increases as hpe increases as shown in figure 3.8. The maximum appears earlier in time as hpe increases. The same trend is also observed for production and dissipation in figure 3.9 and figure 3.10. For hpe = 0.1, the values of energy, production and dissipation remain relatively flat and close to 0.

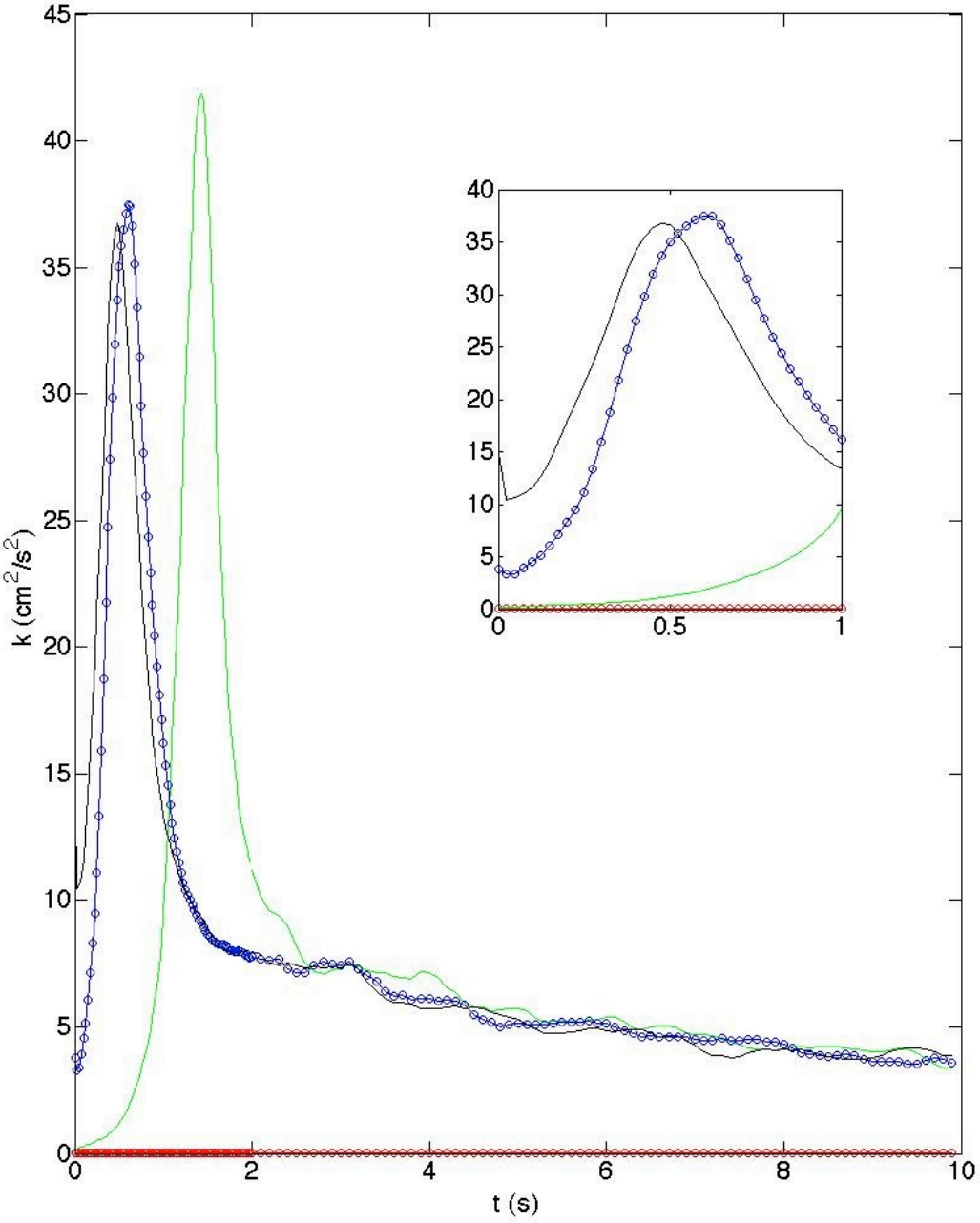

Figure 3.5. Energy for Re = 6000, n = 1.0, crand = 0.001 (hpe: red: 0.1; green: 1; blue: 5; black: 10)

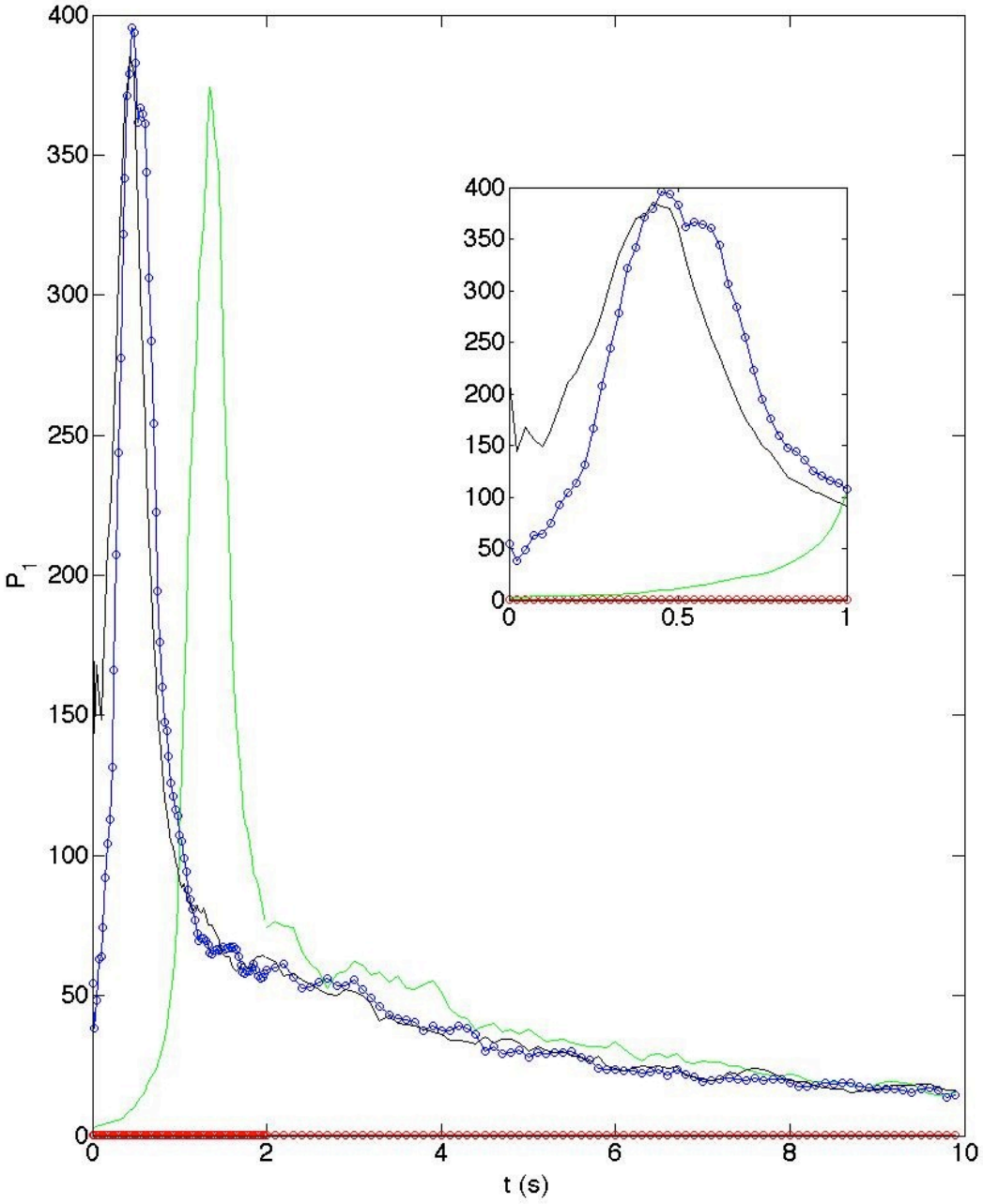

Figure 3.6. Production for Re = 6000, n = 1.0, crand = 0.001 (hpe: red: 0.1; green: 1; blue: 5; black: 10)

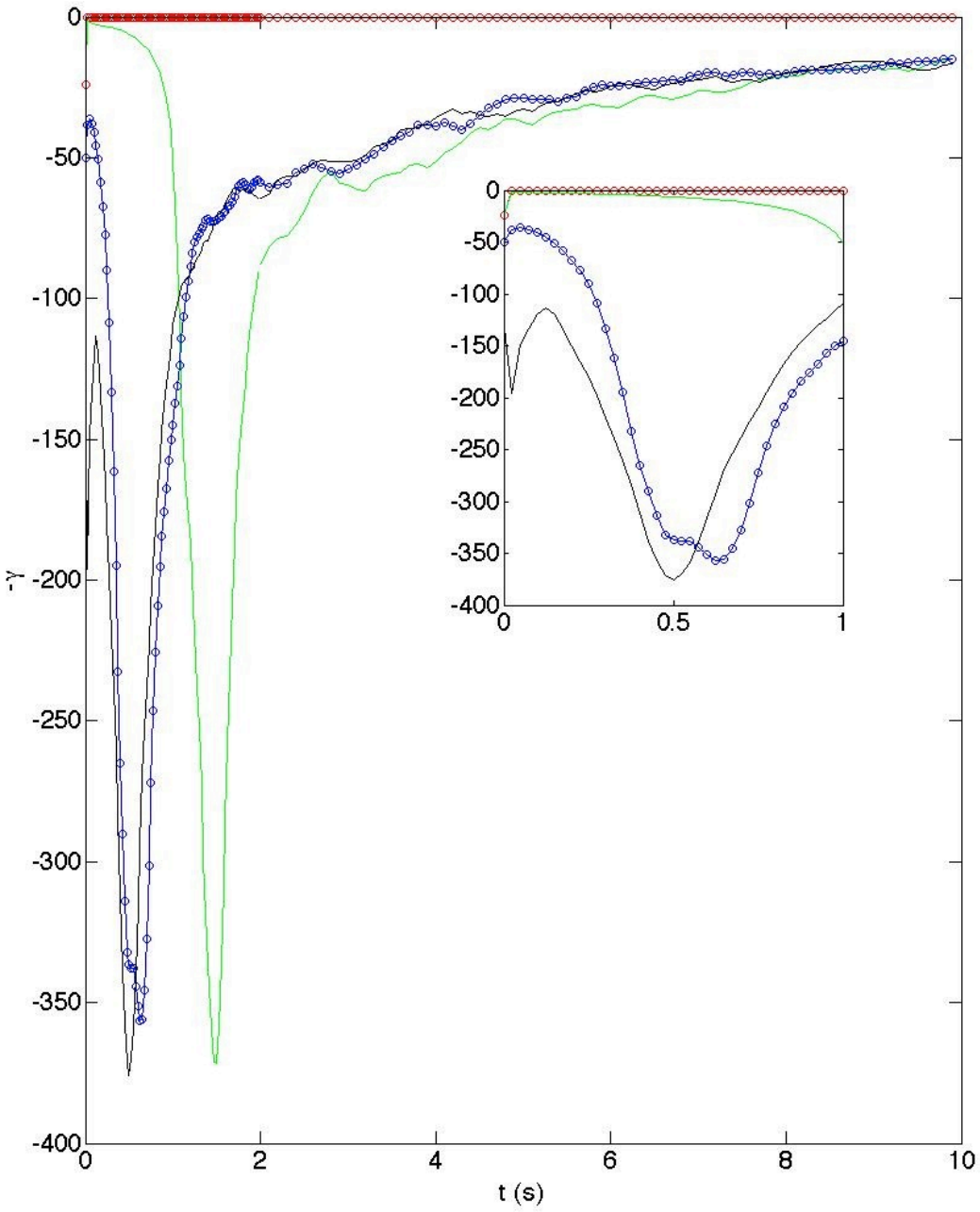

Figure 3.7. Dissipation for Re = 6000, n = 1.0, crand = 0.001 (hpe: red: 0.1; green: 1; blue: 5; black: 10)

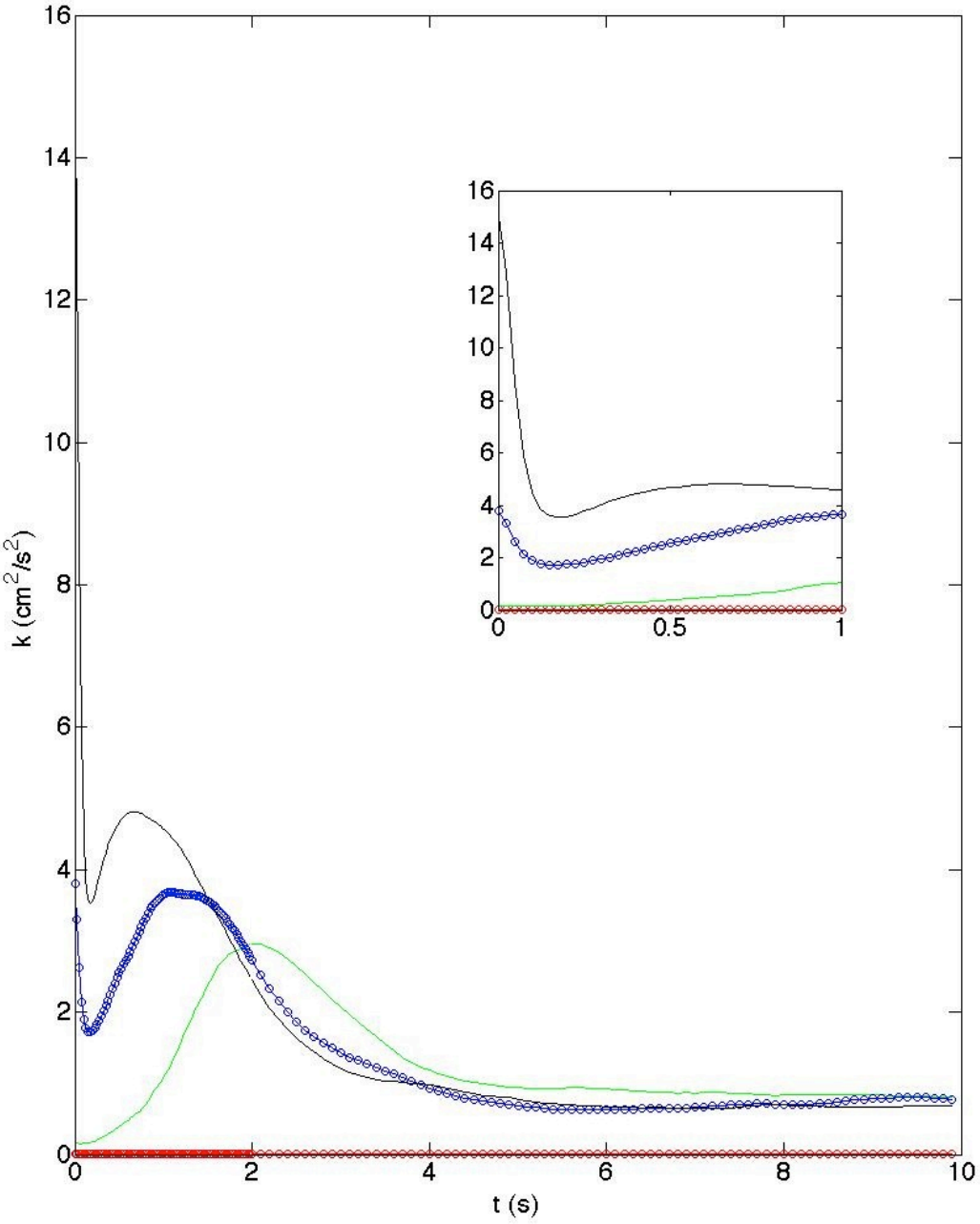

Figure 3.8. Energy for Re = 6000, n = 0.7, crand = 0.001 (hpe: red: 0.1; green: 1; blue: 5; black: 10)

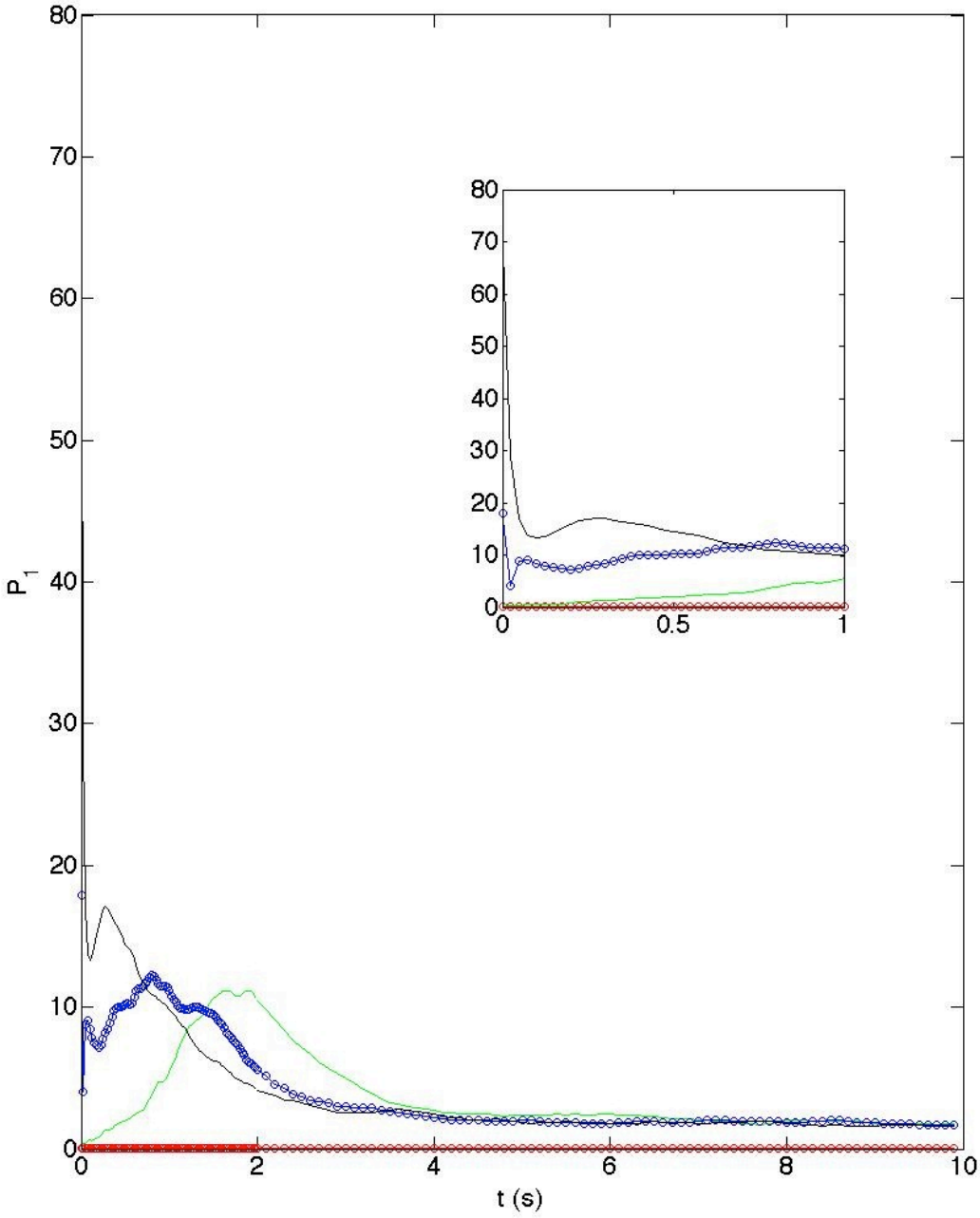

Figure 3.9. Production for Re = 6000, n = 0.7, crand = 0.001 (hpe: red: 0.1; green: 1; blue: 5; black: 10)

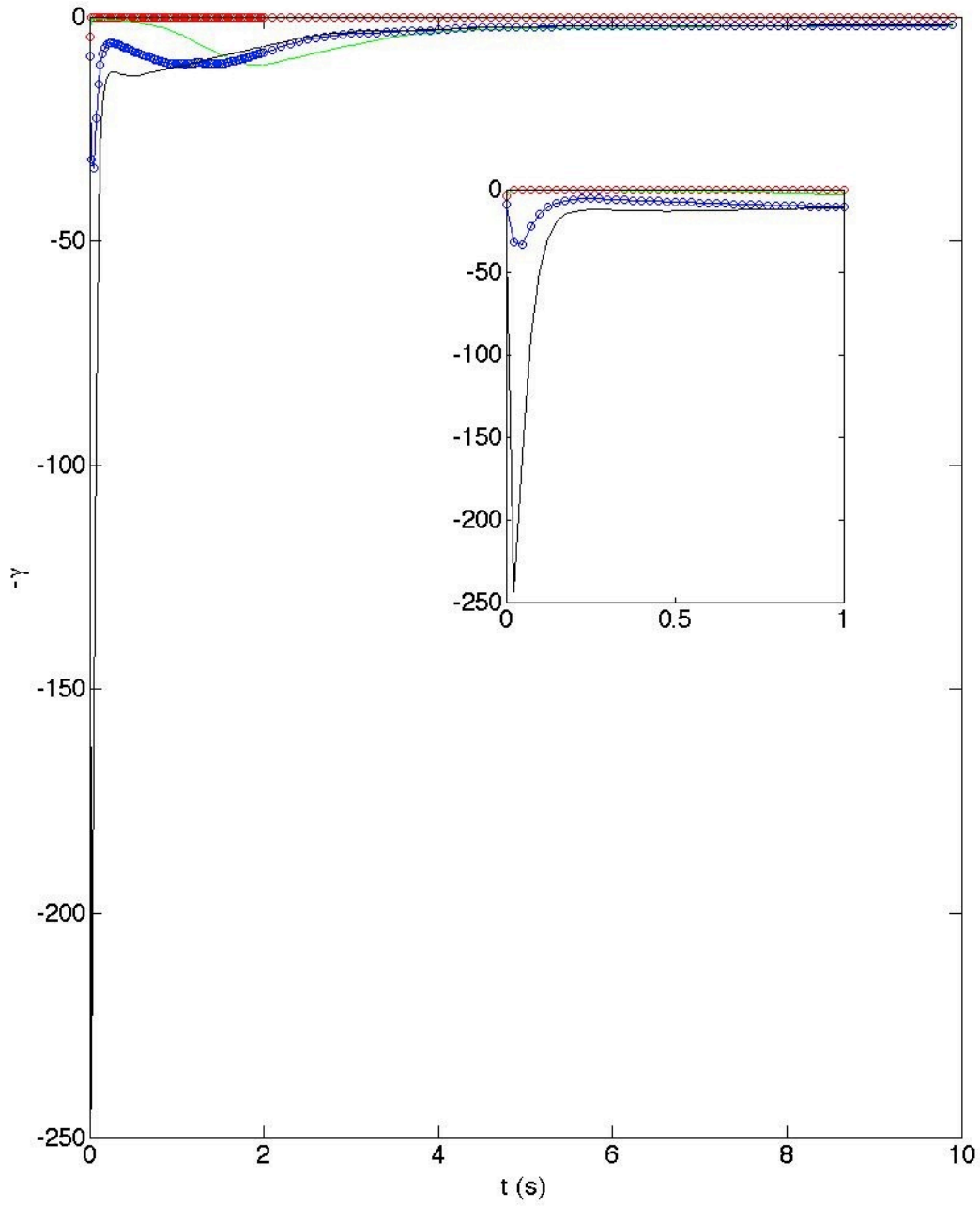

Figure 3.10. dissipation for Re = 6000, n = 0.7, crand = 0.001 (hpe: red: 0.1; green: 1; blue: 5; black: 10)

4. CONCLUSIONS

In this research effort, the effect of a shear thinning fluid governed by a power law model on the evolution of a hairpin vortex was investigated in the channel flow geometry by means of direct numerical simulation. With a fixed Reynolds number based on the initial maximum flow velocity and wall viscosity, the effect of the power law index 'n' on the evolution of the vortex was explored. It was found that very early in time, as the fluid becomes increasingly shear thinning, the dissipation of kinetic energy of the hairpin increases dramatically while the production decreases. Three-dimensional flow visualizations reveal that as shear thinning is increased, the hairpin is prone to a strong instability in which it rapidly loses coherence. This instability is associated with the breakdown of the vortex into small scale structures early in time for the smallest values of 'n', a process which corresponds to increased viscous dissipation.

Experiments cited herein have shown that shear thinning fluids can delay the transition of a flow to turbulence and can also lead to drag reduction. The simulations performed here suggest a possible mechanism for this in which hairpin vortices, a major topological building block of wall-bounded turbulence, are weakened or prevented from forming in a shear thinning fluid as they undergo the instability described in this dissertation. It is unclear, however, what may be causing this instability. It is important to point out that the strength of the hairpin used in this investigation, having an initial kinetic energy which is several percent of the maximum initial flow velocity, is clearly of finite amplitude. In this sense, linear theories (Nouar et al., 2007; Rosenhead, 1963)

are unlikely to be successful in elucidating the flows explored here. In fact, since the hairpin has considerable initial kinetic energy, it seems likely that the strain field generated by the vortex itself may be significantly affecting the local viscosity. In other words, unlike standard linear models in which disturbances passively respond to flow shear or to already present viscosity stratification, here the hairpin vortex itself may be significantly altering the local flow environment.

Flow visualizations reveal a flow in which, due to the relatively high Reynolds numbers, a simple hairpin vortex evolves into a complex, random, vorticity field. Given such complexity, it seems unlikely that a simple explanation for the effects of shear thinning on vortex evolution can easily be found. However, a simple heuristic explanation may be that the rate of strain field generated by the hairpin vortex is sufficient to decrease the viscosity very near the vortex cores, as we would expect from a power law model. If we define a local Reynolds number based on the initial circulation of the flow around the core of the hairpin's leg, and the viscosity 'near' but outside the core, we can expect that this Reynolds number should increase as 'n' is decreased, thereby leading to vortex instability. It is a tentative explanation for the experimental observation. This conjecture will require future studies. It is important to note that in non-Newtonian flows dominated by viscoelasticity (Kim et al., 2008; Kim and Sureshkumar, 2013) it was found that hairpin vortices are suppressed by viscoelastic torques which are directed counter to the vorticity of the hairpin core, thus leading to reduced hairpin strength. Elastic forces inhibit the vortex stretching. Viscoelasticity makes the flow more stable and reduces drag. The authors did not mention dissipation.

For purely shear thinning flows, the mechanism responsible for reducing hairpin strength is quite different as it appears to be associated with the instability of the vortex itself leading to increased viscous dissipation. In (Kim et al., 2008; Kim and Sureshkumar, 2013), hairpins follow slow decay. In this dissertation, hairpins dissipate in a dramatic manner. Visco-elastic fluids are more complicated than shear-thinning fluids.

5. FUTURE WORK

This dissertation work shows that shear-thinning fluids have a strong effect of the evolution of hairpin vortices, and on the transition of laminar flows to turbulent ones. Future work will explore these issues in greater depth and more comprehensively. These tasks include: (1) Exploring the effects of shear-thinning on the statistical properties of fully developed turbulent channel flow, and (2) Investigate the effects of differing viscosity models on the transition process. In task (2), the Carreau model (Cho and Kensey, 1991) will be used in which the fluid viscosity μ is given by:

$$\mu = \mu_\infty + \left(\mu_0 - \mu_\infty\right)\left[1 + \left(\lambda\gamma\right)^2\right]^{(n-1)/2} \qquad (5.1)$$

where μ_∞ is the viscosity at the infinite shear rate, μ_0 is the viscosity at zero shear rate, γ is the shear rate, λ is the relaxation time, and 'n' is the power law index. At low shear rates, Carreau fluids behave as Newtonian fluids whearas at high shear rates they behave as power law fluids. Performing these two simulations will give rise to a much more comprehensive understanding of the effects of shear-thinning fluids on wall-bounded turbulent flows.

We attempted to simulate shear-thickening fluids. It is unclear whether or not shear-thickening will promote transition to turbulence. For future work, the effects of shear-thickening fluids on the evolution of hairpins can be investigated.

REFERENCES

R. J. ADRIAN, "Hairpin Vortex Organization in Wall Turbulence," Physics of Fluids, vol. 19, issue 4, 2007.

G. I. BARENBLATT, A. J. CHORIN and V. M. PROSTOKISHIN, "Scaling Laws for Fully Developed Turbulent Flow in Pipes", Applied Mechanics Reviews, vol. 50, pp. 413-429, 1997.

G. K. BATCHELOR, The Theory of Homogeneous Turbulence, Cambridge University Press, Cambridge, 1953.

P. S. BERNARD, J. M. THOMAS, R. A. HANDLER, "Vortex Dynamics and the Production of Reynolds Stress," Journal of Fluid Mechanics, vol. 253, pp. 385-419, 1993.

R. C. BHATTACHARJEE, N. C. DAS, "Power Law Fluid Model incorporated into Elastohydrodynamic Lubrication Theory of Line Contact," Tribology International, vol. 29, issue 5, pp. 405-413, 1996.

J. W. BROOKE and T. J. HANRATTY, "Origin of Turbulence-Producing Eddies in a Channel Flow," Physics of Fluids A-Fluid Dynamics, vol. 5, pp. 1011–1022, 1993.

R. P. CHHABRA and J. F. RICHARDSON, Non-Newtonian Flow in the Process Industries, Butterworth-Heinemann, Oxford, 1999.

Y. I. CHO and K. R. KENSEY, "Effects of the Non-Newtonian Viscosity of Blood on Flows in a Diseased Arterial Vessel .1. Steady Flows," Biorheology, vol. 28, pp. 241-262, 1991.

A. M. DICKIE and J. L. KOKINI, "An Improved Model for Food Thickness from Non-Newtonian Fluid Mechanics in the Mouth," Journal of Food Science, vol. 48, pp. 57-61, 1983.

M. P. ESCUDIER and F. PRESTI, "Pipe Flow of a Thixotropic Liquid," Journal of Non-Newtonian Fluid Mechanics, vol. 62, pp. 291–306, 1996.

C. A. HIEBER and S. F. SHEN, "A Finite-Element-Finite-Difference Simulation of the Injection-Molding Filling Process," Journal of Non-Newtonian Fluid Mechanics, vol. 7, pp. 1-32, 1980.

J. O. HINZE, Turbulence, McGraw-Hill, New York, 1975.

C. U. IKOKU and H. J. RAMEY Jr., "Transient Flow of Non-Newtonian Power-Law Fluids in Porous-Media," Society of Petroleum Engineers Journal, vol. 19, pp. 164-174, 1979.

J. JEONG, F. HUSSAIN, “On the Identification of a Vortex,” Journal of Fluid Mechanics, vol. 285, pp. 69-94, 1995.

B. M. JOHNSTON, P. R. JOHNSTON, S. Corney and D. Kilpatrick, "Non-Newtonian Blood Flow in Human Right Coronary Arteries: Steady State Simulations," Journal of Biomechanics, vol. 37, pp. 709–720, 2004.

T. VON KARMAN, “The Fundamentals of the Statistical Theory of Turbulence”, Journal of the Aeronautical Sciences, vol. 4, pp. 131-138, 1937.

K. KIM, R. J. ADRIAN, S. BALACHANDAR and R. SURESHKUMAR, "Dynamics of Hairpin Vortices and Polymer-Induced Drag Reduction," Physical Review Letters, vol. 100, 2008.

J. KIM, P. MOIN and R. MOSER, "Turbulent Statistics in Fully Developed Channel Flow at Low Reynolds Number," Journal of Fluid Mechanics, vol. 177, pp. 133-166, 1987.

K. KIM and R. SURESHKUMAR, “Spatiotemporal Evolution of Hairpin Eddies, Reynolds stress, and Polymer Torque in Polymer Drag-reduced Turbulent Channel Flows”, Physical Review E, vol. 87, issue. 6, 2013.

S. J. KLINE, W. C. REYNOLDS, F. A. SCHRAUB and P. W. RUNSTADLER, "The Structure of Turbulent Boundary Layers," Journal of Fluid Mechanics, vol. 30, pp.741-773, 1967.

C. LANCZOS, Applied Analysis, Prentice-Hall, 1956.

C. C. LIN, Statistical Theories of Turbulence, Princeton University Press, 1961.

J. L. LUMLEY, "Drag Reduction by Additives," Annual Review of Fluid Mechanics, vol. 1, 1969.

J. L. LUMLEY, "Drag Reduction in Turbulent Flow by Polymer Additives," Journal of Polymer Science Macromolecular Reviews, vol. 7, pp. 263-290, 1973.

J. MEWIS, "Thixotropy - General-Review," Journal of Non-Newtonian Fluid Mechanics, vol. 6, pp. 1-20, 1979.

P. MOIN and J. KIM, "On the Numerical-Solution of Time-Dependent Viscous Incompressible Fluid-Flows Involving Solid Boundaries," Journal of Computational Physics, vol. 35, pp. 381-392, 1980.

P. MOIN and J. KIM, "Numerical Investigation of Turbulent Channel Flow," Journal of Fluid Mechanics, vol. 118, pp. 341-377, 1982.

C. NOUAR, A. BOTTARO and J. P. BRANCHER, "Delaying Transition to Turbulence in Channel Flow: Revisiting the Stability of Shear-Thinning Fluids," Journal of Fluid Mechanics, vol. 592, pp. 177-194, 2007.

S. A. ORSZAG, "Accurate Solution of Orr-Sommerfeld Stability Equation," Journal of Fluid Mechanics, vol. 50, pp. 659-703, 1971.

J. T. PARK, R. J. MANNHEIMER, T. A. GRIMLEY and T. B. MORROW, "Pipe Flow Measurements of a Transparent Non-Newtonian Slurry," Journal of Fluids Engineering, vol. 111, pp. 331-336, 1989.

F. T. PINHO, and J. H. WHITELAW, "Flow of Non-Newtonian Fluids in a Pipe," Journal of Non-Newtonian Fluid Mechanics, vol. 34, pp. 129-144, 1990.

K. K. RAJU, R. DEVANATHAN, "Peristaltic Motion of a non-Newtonian Fluid," Rheologica Acta, vol. 13, pp. 944-948, 1974.

S. K. ROBINSON, "Coherent Motions in the Turbulent Boundary Layer," Annual Review of Fluid Mechanics, vol. 23, pp. 601-639, 1991.

L. ROSENHEAD, Laminar Boundary Layers, Oxford University Press, 1963.

M. RUDMAN, H. M. BLACKBURN, L. J. W. GRAHAM and L. PULLUM, "Turbulent Pipe flow of Shear-Thinning Fluids," Journal of Non-Newtonian Fluid Mechanics, vol. 118, pp. 33-48, 2004.

P. SINHA, J. B. SHUKLA, K. R. PRASAD and C. SINGH, "Non-Newtonian Power Law Fluid Lubrication of Lightly Loaded Cylinders with Normal and Rolling Motion," Wear, vol. 89, pp. 313-322, 1983.

C. R. SMITH and S. P. METZLER, "Characteristics of Low-Speed Streaks in the near-Wall Region of a Turbulent Boundary Layer," Journal of Fluid Mechanics, vol. 129, pp. 27-54, 1983.

L. M. SRIVASTAVA and V. P. SRIVASTAVA, "Peristalic Transport of a non-Newtonian Fluid: Applications to the Vas Deferens and Small Intestine," Annals of Biomedical Engineering, vol. 13, pp. 137-153, 1985.

J. S. STRAND and D. B. GOLDSTEIN, "Direct Numerical Simulations of Riblets to Constrain the Growth of Turbulent Spots," Journal of Fluid Mechanics, vol. 688, pp. 267-292, 2011.

R. SURESHKUMAR, A. N. BERIS and R. A. HANDLER, "Direct Numerical Simulation of the Turbulent Channel Flow of a Polymer Solution", Physics of Fluids, vol. 9, pp. 743-755, 1997.

R. I. TANNER, Engineering Rheology, Oxford University Press, 1988.

G. I. TAYLOR, "Statistical Theory of Turbulence", Proceedings of Royal Society London A, vol. 151, pp. 421-444, 1935.

H. TENNEKES and J.L. LUMLEY, A First Course in Turbulence, MIT Press, Cambridge, 1972.

T. THEODORSEN, Mechanism of Turbulence, Proceedings of the Second Midwestern Conference of Fluid Mechanics, pp. 1-19. Ohio State University, Columbus, Ohio, 1952.

B. A. TOMS, Proceedings of the 1st International Congress of Rheology, 2, 135-41, North Holland, Amsterdam, 1948.

R. W. VEATCH Jr., "Overview of Current Hydraulic Fracturing Design and Treatment Technology .2.," Journal of Petroleum Technology, vol. 35, pp. 853-864, 1983.

G. VERREET and J. BERLAMONT, in Encyclopedia of Fluid Mechanics, Rheology and Non-Newtonian Flows, edited by N.P. Cheremisinoff, Gulf Publishing Company, Houston, vol. 7, p. 135, 1988.

N. ZHEN, R. HANDLER, Q. ZHANG, C. OETH, “Evolution of a Hairpin Vortex in a Shear-Thinning Fluid Governed by Power-Law Model,” Physics of Fluids, vol. 25, no. 10, 2013.

J. ZHOU, R. J. ADRIAN, S. BALACHANDAR and T. M. KENDALL, "Mechanisms for Generating Coherent Packets of Hairpin Vortices in Channel," Journal of Fluid Mechanics, vol. 387, pp. 353-396, 1999.

APPENDIX A: DERIVATION OF THE TURBULENT KINETIC ENERGY EQUATION

A.1 Derivation of the Kinetic Energy Equation for a Newtonian Flow

A.1.1 Newtonian flow during Transient

The notion used in all derivations in Appendix A is the same as the notion used in Section 3.2 of (Tennekes and Lumley, 1972). $\bar{}$ means ensemble average. The ensemble average of a fluctuating quantity is zero while the ensemble average of an average quantity is the variable itself.

The equation of motion of an incompressible fluid is:

$$\frac{\partial V_i}{\partial t} + V_j \partial_j V_i = -\partial_i \frac{P}{\rho} + \nu \partial_j \partial_j V_i \qquad (A.1)$$

The velocity V_i is decomposed into ensemble average U_i and velocity fluctuation u_i, such that

$$V_i = U_i + u_i \qquad (A.2)$$

The pressure P is also decomposed into ensemble average and fluctuating components.

$$P = \overline{P} + p \qquad (A.3)$$

In the derivations in Section A.1.1 and Section A.1.2, ν is the Newtonian kinematic viscosity.

We multiply each term of the equation of motion by velocity fluctuation u_k and obtain the ensemble average of every individual term:

Unsteady term:

$$\overline{u_k \frac{\partial V_i}{\partial t}} = \overline{u_k \frac{\partial (U_i + u_i)}{\partial t}} = \overline{u_k \frac{\partial u_i}{\partial t}} \qquad (A.4)$$

Convective term:

$$\overline{u_k (U_j + u_j) \partial_j (U_i + u_i)} = \overline{u_k U_j \partial_j U_i + u_k U_j \partial_j u_i + u_k u_j \partial_j U_i + u_k u_j \partial_j u_i}$$

$$= \overline{u_k U_j \partial_j u_i + u_k u_j \partial_j U_i + u_k u_j \partial_j u_i} = \overline{u_k U_j \partial_j u_i} + \overline{u_k u_j \partial_j U_i} + \overline{u_k u_j \partial_j u_i} \qquad (A.5)$$

Pressure term:

$$\overline{u_k \partial_i \frac{P}{\rho}} = \overline{u_k \partial_i \frac{(\overline{P} + p)}{\rho}} = \overline{u_k \partial_i \frac{p}{\rho}} \qquad (A.6)$$

Viscous term:

$$\overline{u_k \nu \partial_j \partial_j V_i} = \overline{\nu u_k \partial_j \partial_j (U_i + u_i)} = \overline{\nu u_k \partial_j \partial_j u_i} \qquad (A.7)$$

We add $(A.4)(A.5)(A.6)(A.7)$ and obtain the ensemble average of $(A.1)$:

$$\overline{u_k \frac{\partial u_i}{\partial t}} + \overline{u_k U_j \partial_j u_i + u_k u_j \partial_j U_i + u_k u_j \partial_j u_i} = \overline{-u_k \partial_i \frac{p}{\rho}} + \overline{\nu u_k \partial_j \partial_j u_i}$$

$$\overline{u_k \frac{\partial u_i}{\partial t}} + U_j \overline{u_k \partial_j u_i} + \overline{u_k u_j} \partial_j U_i + \overline{u_k u_j \partial_j u_i} = \overline{-u_k \partial_i \frac{p}{\rho}} + \nu \overline{u_k \partial_j \partial_j u_i} \qquad (A.8)$$

We switch i and k in $(A.8)$ which results in $(A.9)$:

$$\overline{u_i \frac{\partial u_k}{\partial t}} + U_j \overline{u_i \partial_j u_k} + \overline{u_i u_j} \partial_j U_k + \overline{u_i u_j \partial_j u_k} = \overline{-u_i \partial_k \frac{p}{\rho}} + \nu \overline{u_i \partial_j \partial_j u_k} \qquad (A.9)$$

We add $(A.8)$ and $(A.9)$:

$$\overline{u_k \frac{\partial u_i}{\partial t}} + \overline{u_i \frac{\partial u_k}{\partial t}} + U_j \left(\overline{u_k \partial_j u_i} + \overline{u_i \partial_j u_k} \right) + \overline{u_k u_j} \partial_j U_i + \overline{u_k u_j \partial_j u_i} + \overline{u_i u_j} \partial_j U_k + \overline{u_i u_j \partial_j u_k}$$

$$= \overline{-u_k \partial_i \frac{p}{\rho}} - \overline{u_i \partial_k \frac{p}{\rho}} + \nu \left(\overline{u_k \partial_j \partial_j u_i} + \overline{u_i \partial_j \partial_j u_k} \right) \qquad (A.10)$$

We apply chain rule to each term of $(A.10)$ except for $\overline{u_k u_j} \partial_j U_i$, $\overline{u_i u_j} \partial_j U_k$ and pressure terms:

Unsteady terms:

$$\overline{\frac{\partial u_i u_k}{\partial t}} = \overline{u_i \frac{\partial u_k}{\partial t}} + \overline{u_k \frac{\partial u_i}{\partial t}} \qquad (A.11)$$

Convective terms:

$$U_j \overline{\partial_j u_i u_k} = U_j \left(\overline{u_k \partial_j u_i} + \overline{u_i \partial_j u_k} \right) \qquad (A.12)$$

$$\overline{\partial_j \left(u_i u_j u_k \right)} = \overline{u_i \partial_j \left(u_j u_k \right)} + \overline{\left(u_j u_k \right) \partial_j u_i}$$

$$= \overline{u_i \left(u_j \partial_j u_k + u_k \partial_j u_j \right)} + \overline{u_j u_k \partial_j u_i} = \overline{u_i u_j \partial_j u_k} + \overline{u_j u_k \partial_j u_i} \qquad (A.13)$$

Viscous terms:

$$\overline{u_k \partial_j \partial_j u_i} + \overline{u_i \partial_j \partial_j u_k} = B$$

$$\overline{\partial_j \partial_j \left(u_i u_k \right)} = \partial_j \left(\overline{u_i \partial_j u_k} + \overline{u_k \partial_j u_i} \right)$$

$$= \overline{\partial_j u_i \partial_j u_k} + \overline{u_i \partial_j \partial_j u_k} + \overline{\partial_j u_k \partial_j u_i} + \overline{u_k \partial_j \partial_j u_i} = B + \overline{2 \partial_j u_i \partial_j u_k}$$

$$\nu \left(\overline{u_k \partial_j \partial_j u_i} + \overline{u_i \partial_j \partial_j u_k} \right) = \nu \left[\overline{\partial_j \partial_j \left(u_i u_k \right)} - 2 \overline{\frac{\partial u_i}{\partial x_j} \frac{\partial u_k}{\partial x_j}} \right] \qquad (A.14)$$

We obtain $(A.15)$:

$$\overline{\frac{\partial u_i u_k}{\partial t}} + U_j \frac{\partial}{\partial x_j} \overline{u_i u_k}$$

$$= -\overline{u_k u_j} \frac{\partial U_i}{\partial x_j} - \overline{u_i u_j} \frac{\partial U_k}{\partial x_j} - \frac{\partial \overline{\left(u_i u_j u_k \right)}}{\partial x_j} - \overline{u_k \frac{\partial \frac{p}{\rho}}{\partial x_i}} - \overline{u_i \frac{\partial \frac{p}{\rho}}{\partial x_k}} + \nu \frac{\partial^2}{\partial^2 x_j} \overline{u_i u_k} - 2\nu \overline{\frac{\partial u_i}{\partial x_j} \frac{\partial u_k}{\partial x_j}} +$$

buoyancy terms $\qquad (A.15)$

Convective derivative of the Reynolds stress: $U_j \frac{\partial}{\partial x_j} \overline{u_i u_k}$

Production: $-\overline{u_k u_j} \frac{\partial U_i}{\partial x_j} - \overline{u_i u_j} \frac{\partial U_k}{\partial x_j}$

Turbulent transport: $-\frac{\partial \overline{\left(u_i u_j u_k \right)}}{\partial x_j}$

Pressure transport: $-\overline{u_k \frac{\partial \frac{p}{\rho}}{\partial x_i}} - \overline{u_i \frac{\partial \frac{p}{\rho}}{\partial x_k}}$

Diffusion: $\nu \frac{\partial^2}{\partial^2 x_j} \overline{u_i u_k}$

Dissipation: $\mathrm{E}_{ij} = -2\nu \overline{\frac{\partial u_i}{\partial x_j} \frac{\partial u_k}{\partial x_j}}$

Isotropic dissipation: $\mathrm{E}_s = \frac{\mathrm{E}_{ii}}{2} = \nu \left(\frac{\partial u_i}{\partial x_j} \right)^2$

We take the trace of $(A.15)$:

$$\delta_{ik} \left[\frac{\partial \overline{u_i u_k}}{\partial t} + U_j \frac{\partial}{\partial x_j} \overline{u_i u_k} \right]$$

$$= \delta_{ik} \left[-\overline{u_k u_j} \frac{\partial U_i}{\partial x_j} - \overline{u_i u_j} \frac{\partial U_k}{\partial x_j} - \frac{\partial \overline{\left(u_i u_j u_k \right)}}{\partial x_j} - \overline{u_k \frac{\partial \frac{p}{\rho}}{\partial x_i}} - \overline{u_i \frac{\partial \frac{p}{\rho}}{\partial x_k}} + \nu \frac{\partial^2}{\partial^2 x_j} \overline{u_i u_k} - 2\nu \overline{\frac{\partial u_i}{\partial x_j} \frac{\partial u_k}{\partial x_j}} \right]$$

$$\frac{\partial \overline{u_i u_i}}{\partial t} + U_j \frac{\partial}{\partial x_j} \overline{u_i u_i}$$

$$= -\overline{u_i u_j} \frac{\partial U_i}{\partial x_j} - \overline{u_i u_j} \frac{\partial U_i}{\partial x_j} - \frac{\partial \overline{\left(u_i u_j u_i \right)}}{\partial x_j} - \overline{u_i \frac{\partial \frac{p}{\rho}}{\partial x_i}} - \overline{u_i \frac{\partial \frac{p}{\rho}}{\partial x_i}} + \nu \frac{\partial^2}{\partial^2 x_j} \overline{u_i u_i} - 2\nu \overline{\frac{\partial u_i}{\partial x_j} \frac{\partial u_i}{\partial x_j}}$$

$$\frac{\partial \overline{u_i u_i}}{\partial t} + U_j \frac{\partial}{\partial x_j} \overline{u_i u_i} = -2\overline{u_i u_j} \frac{\partial U_i}{\partial x_j} - \frac{\partial \overline{\left(u_i u_j u_i \right)}}{\partial x_j} - 2\overline{u_i \frac{\partial \frac{p}{\rho}}{\partial x_i}} + \nu \frac{\partial^2}{\partial^2 x_j} \overline{u_i u_i} - 2\nu \overline{\frac{\partial u_i}{\partial x_j} \frac{\partial u_i}{\partial x_j}}$$

We then have the final form of the kinetic equation for a fully developed turbulent flow as the following:

$$\frac{1}{2}\frac{\partial\overline{u_i u_i}}{\partial t}+\frac{1}{2}U_j\frac{\partial}{\partial x_j}\overline{u_i u_i}$$

$$=-\overline{u_i u_j}\frac{\partial U_i}{\partial x_j}-\frac{1}{2}\frac{\partial\overline{\left(u_i u_j u_i\right)}}{\partial x_j}-\overline{u_i\frac{\partial\frac{p}{\rho}}{\partial x_i}}+\frac{1}{2}\nu\frac{\partial^2}{\partial^2 x_j}\overline{u_i u_i}-\nu\overline{\frac{\partial u_i}{\partial x_j}\frac{\partial u_i}{\partial x_j}} \qquad (A.16)$$

A.1.2 Newtonian flow during transient

The symmetric part of the velocity gradient tensor Σ_{ij} is decomposed into an average quantity S_{ij} and fluctuation s_{ij} such that:

$$\Sigma_{ij}=S_{ij}+s_{ij} \qquad (A.17)$$

$$S_{ij}=\frac{1}{2}\left(\frac{\partial U_i}{\partial x_j}+\frac{\partial U_j}{\partial x_i}\right)$$

$$2\nu\frac{\partial}{\partial x_j}S_{ij}=\nu\frac{\partial}{\partial x_j}\left(\frac{\partial U_i}{\partial x_j}+\frac{\partial U_j}{\partial x_i}\right)$$

$$=\nu\frac{\partial}{\partial x_j}\frac{\partial U_i}{\partial x_j}+\nu\frac{\partial}{\partial x_j}\frac{\partial U_j}{\partial x_i}=\nu\frac{\partial}{\partial x_j}\frac{\partial U_i}{\partial x_j}+\nu\frac{\partial}{\partial x_i}\frac{\partial U_j}{\partial x_j}=\nu\frac{\partial}{\partial x_j}\frac{\partial U_i}{\partial x_j}$$

$$s_{ij}=\frac{1}{2}\left(\frac{\partial u_i}{\partial x_j}+\frac{\partial u_j}{\partial x_i}\right)$$

$$2\nu\frac{\partial}{\partial x_j}s_{ij}=\nu\frac{\partial}{\partial x_j}\left(\frac{\partial u_i}{\partial x_j}+\frac{\partial u_j}{\partial x_i}\right)$$

$$=\nu\frac{\partial}{\partial x_j}\frac{\partial u_i}{\partial x_j}+\nu\frac{\partial}{\partial x_j}\frac{\partial u_j}{\partial x_i}=\nu\frac{\partial}{\partial x_j}\frac{\partial u_i}{\partial x_j}+\nu\frac{\partial}{\partial x_i}\frac{\partial u_j}{\partial x_j}=\nu\frac{\partial}{\partial x_j}\frac{\partial u_i}{\partial x_j}$$

$$\nu\frac{\partial}{\partial x_j}\frac{\partial U_i}{\partial x_j}+\nu\frac{\partial}{\partial x_j}\frac{\partial u_i}{\partial x_j}=\nu\partial_j\partial_j V_i=2\nu\frac{\partial}{\partial x_j}S_{ij}+2\nu\frac{\partial}{\partial x_j}s_{ij}=2\nu\frac{\partial}{\partial x_j}\Sigma_{ij} \qquad (A.18)$$

The equation of motion of an incompressible fluid then becomes $(A.19)$:

$$\frac{\partial V_i}{\partial t}+V_j\partial_j V_i=-\partial_i\frac{P}{\rho}+2\nu\partial_j\Sigma_{ij} \qquad (A.19)$$

We multiply the viscous term by velocity fluctuation u_k and obtain the ensemble average:

$$\overline{u_k 2\nu\partial_j\Sigma_{ij}}=\overline{2\nu u_k\partial_j\Sigma_{ij}}=2\nu\overline{u_k\partial_j\left(S_{ij}+s_{ij}\right)}=2\nu\overline{u_k\partial_j s_{ij}} \qquad (A.20)$$

We then have the ensemble average of $(A.19)$:

$$\overline{u_k\frac{\partial u_i}{\partial t}}+U_j\overline{u_k\partial_j u_i}+\overline{u_k u_j}\partial_j U_i+\overline{u_k u_j\partial_j u_i}=-\overline{u_k\partial_i\frac{p}{\rho}}+2\nu\overline{u_k\partial_j s_{ij}} \qquad (A.21)$$

We switch i and k, we then obtain $(A.22)$:

$$\overline{u_i\frac{\partial u_k}{\partial t}}+U_j\overline{u_i\partial_j u_k}+\overline{u_i u_j}\partial_j U_k+\overline{u_i u_j\partial_j u_k}=-\overline{u_i\partial_k\frac{p}{\rho}}+2\nu\overline{u_i\partial_j s_{kj}} \qquad (A.22)$$

We add $(A.21)$ and $(A.22)$:

$$\overline{u_k\frac{\partial u_i}{\partial t}}+\overline{u_i\frac{\partial u_k}{\partial t}}+U_j\left(\overline{u_k\partial_j u_i}+\overline{u_i\partial_j u_k}\right)+\overline{u_k u_j}\partial_j U_i+\overline{u_k u_j\partial_j u_i}+\overline{u_i u_j}\partial_j U_k+\overline{u_i u_j\partial_j u_k}$$

$$=-\overline{u_k\partial_i\frac{p}{\rho}}-\overline{u_i\partial_k\frac{p}{\rho}}+2\nu\left(\overline{u_k\partial_j s_{ij}}+\overline{u_i\partial_j s_{kj}}\right) \qquad (A.23)$$

We then obtain $(A.24)$:

$$\frac{\partial\overline{u_i u_k}}{\partial t}+U_j\frac{\partial}{\partial x_j}\overline{u_i u_k}$$

$$=-\overline{u_k u_j}\frac{\partial U_i}{\partial x_j}-\overline{u_i u_j}\frac{\partial U_k}{\partial x_j}-\frac{\partial\left(\overline{u_i u_j u_k}\right)}{\partial x_j}-\overline{u_k\frac{\partial\frac{p}{\rho}}{\partial x_i}}-\overline{u_i\frac{\partial\frac{p}{\rho}}{\partial x_k}}+2\nu\left(\overline{u_k\partial_j s_{ij}}+\overline{u_i\partial_j s_{kj}}\right)+$$

buoyancy terms $(A.24)$

We take the trace of $(A.24)$:

$$\delta_{ik}\left[\frac{\partial\overline{u_i u_k}}{\partial t}+U_j\frac{\partial}{\partial x_j}\overline{u_i u_k}\right]$$

$$=\delta_{ik}\left[-\overline{u_k u_j}\frac{\partial U_i}{\partial x_j}-\overline{u_i u_j}\frac{\partial U_k}{\partial x_j}-\frac{\partial\left(\overline{u_i u_j u_k}\right)}{\partial x_j}-\overline{u_k\frac{\partial\frac{p}{\rho}}{\partial x_i}}-\overline{u_i\frac{\partial\frac{p}{\rho}}{\partial x_k}}+2\nu\left(\overline{u_k\partial_j s_{ij}}+\overline{u_i\partial_j s_{kj}}\right)\right]$$

$$\frac{\partial\overline{u_i u_i}}{\partial t}+U_j\frac{\partial}{\partial x_j}\overline{u_i u_i}$$

$$=-\overline{u_i u_j}\frac{\partial U_i}{\partial x_j}-\overline{u_i u_j}\frac{\partial U_i}{\partial x_j}-\frac{\partial\left(\overline{u_i u_j u_i}\right)}{\partial x_j}-\overline{u_i\frac{\partial\frac{p}{\rho}}{\partial x_i}}-\overline{u_i\frac{\partial\frac{p}{\rho}}{\partial x_i}}+2\nu\left(\overline{u_i\partial_j s_{ij}}+\overline{u_i\partial_j s_{ij}}\right)$$

$$\frac{\partial\overline{u_i u_i}}{\partial t}+U_j\frac{\partial}{\partial x_j}\overline{u_i u_i}=-2\overline{u_i u_j}\frac{\partial U_i}{\partial x_j}-\frac{\partial\left(\overline{u_i u_j u_i}\right)}{\partial x_j}-2\overline{u_i\frac{\partial\frac{p}{\rho}}{\partial x_i}}+4\nu\overline{u_i\partial_j s_{ij}} \qquad (A.25)$$

We switch the dummy indices i and j in $\overline{u_i u_j}\frac{\partial U_i}{\partial x_j}$:

$$\overline{u_i u_j}\frac{\partial U_i}{\partial x_j}=\overline{u_j u_i}\frac{\partial U_j}{\partial x_i}=\overline{u_i u_j}\frac{\partial U_j}{\partial x_i}$$

$$2\overline{u_i u_j}\frac{\partial U_i}{\partial x_j}=\overline{u_i u_j}\frac{\partial U_i}{\partial x_j}+\overline{u_i u_j}\frac{\partial U_j}{\partial x_i}=\overline{u_i u_j}\left(\frac{\partial U_i}{\partial x_j}+\frac{\partial U_j}{\partial x_i}\right)=2\overline{u_i u_j}S_{ij}$$

$$\overline{u_i u_j}\frac{\partial U_i}{\partial x_j}=\overline{u_i u_j}S_{ij} \qquad (A.26)$$

We then use chain rule:

$$4\nu\frac{\partial}{\partial x_j}\overline{u_i s_{ij}}=4\nu\overline{u_i\frac{\partial s_{ij}}{\partial x_j}}+4\nu\overline{s_{ij}\frac{\partial u_i}{\partial x_j}}$$

s_{ij} is symmetric, therefore: $s_{ij}=s_{ji}$. We switch the dummy indices i and j in $\overline{s_{ij}\frac{\partial u_i}{\partial x_j}}$:

$$4\nu\overline{s_{ij}\frac{\partial u_i}{\partial x_j}} = 2\nu\overline{s_{ij}\frac{\partial u_i}{\partial x_j}} + 2\nu\overline{s_{ji}\frac{\partial u_j}{\partial x_i}} = 2\nu\overline{s_{ij}\frac{\partial u_i}{\partial x_j}} + 2\nu\overline{s_{ij}\frac{\partial u_j}{\partial x_i}} = 4\nu\overline{s_{ij}s_{ij}}$$

$$4\nu\overline{u_i\partial_j s_{ij}} = 4\nu\frac{\partial}{\partial x_j}\overline{u_i s_{ij}} - 4\nu\overline{s_{ij}s_{ij}} \qquad (A.27)$$

$$\frac{\partial\overline{u_i u_i}}{\partial t} + U_j\frac{\partial}{\partial x_j}\overline{u_i u_i} = -2\overline{u_i u_j}S_{ij} - \frac{\partial\overline{\left(u_i u_j u_i\right)}}{\partial x_j} - 2u_i\overline{\frac{\partial\frac{p}{\rho}}{\partial x_i}} + 4\nu\frac{\partial}{\partial x_j}\overline{u_i s_{ij}} - 4\nu\overline{s_{ij}s_{ij}}$$

We then have the final form of the kinetic energy equation for a Newtonian flow during transient as the following:

$$\frac{1}{2}\frac{\partial\overline{u_i u_i}}{\partial t} + \frac{1}{2}U_j\frac{\partial}{\partial x_j}\overline{u_i u_i} = -\overline{u_i u_j}S_{ij} - \frac{1}{2}\frac{\partial\overline{\left(u_i u_j u_i\right)}}{\partial x_j} - \overline{u_j\frac{\partial\frac{p}{\rho}}{\partial x_j}} + 2\nu\frac{\partial}{\partial x_j}\overline{u_i s_{ij}} - 2\nu\overline{s_{ij}s_{ij}} \qquad (A.28)$$

$\frac{1}{2}\frac{\partial\overline{u_i u_i}}{\partial t} = 0$ under steady state.

$\overline{\frac{\partial u_j}{\partial x_j}} = 0$ due to continuity.

$$\frac{\partial}{\partial x_j}\frac{1}{\rho}\overline{u_j p} = \frac{1}{\rho}\overline{\frac{\partial u_j}{\partial x_j}p} + \overline{u_j\frac{\partial\frac{p}{\rho}}{\partial x_j}} = \overline{u_j\frac{\partial\frac{p}{\rho}}{\partial x_j}}$$

We then have the kinetic energy equation under steady state:
$U_j\frac{\partial}{\partial x_j}\left(\frac{1}{2}\overline{u_i u_i}\right) = -\frac{\partial}{\partial x_j}\left(\frac{1}{\rho}\overline{u_j p} + \frac{1}{2}\overline{u_i u_i u_j} - 2\nu\overline{u_i s_{ij}}\right) - \overline{u_i u_j}S_{ij} - 2\nu\overline{s_{ij}s_{ij}}$ which is the same as (3.2.1) on page 63 of (Tennekes and Lumley, 1972).

A.2 The Derivation of the Kinetic Equation for a Non-Newtonian Flow during Transient

η is the non-Newtonian kinematic viscosity. The equation of motion of a Non-Newtonian fluid is:

$$\frac{\partial V_i}{\partial t} + V_j \partial_j V_i = -\partial_i \frac{P}{\rho} + \frac{\partial}{\partial x_j}\left(2\eta \Sigma_{ij}\right) \qquad (A.29)$$

We multiply the viscous term by velocity fluctuation u_k and obtain the ensemble average:

$$\overline{u_k \partial_j 2\eta\Sigma_{ij}} = \overline{2u_k \partial_j \eta\Sigma_{ij}} = 2\overline{u_k \partial_j \eta\left(S_{ij} + s_{ij}\right)} = 2\overline{u_k \partial_j \eta S_{ij}} + 2\overline{u_k \partial_j \eta s_{ij}} \qquad (A.30)$$

We then have the ensemble average of $(A.29)$:

$$\overline{u_k \frac{\partial u_i}{\partial t}} + U_j \overline{u_k \partial_j u_i} + \overline{u_k u_j} \partial_j U_i + \overline{u_k u_j \partial_j u_i} = -\overline{u_k \partial_i \frac{p}{\rho}} + 2\overline{u_k \partial_j \eta S_{ij}} + 2\overline{u_k \partial_j \eta s_{ij}} \qquad (A.31)$$

We switch i and k, we then obtain $(A.32)$:

$$\overline{u_i \frac{\partial u_k}{\partial t}} + U_j \overline{u_i \partial_j u_k} + \overline{u_i u_j} \partial_j U_k + \overline{u_i u_j \partial_j u_k} = -\overline{u_i \partial_k \frac{p}{\rho}} + 2\overline{u_i \partial_j \eta S_{kj}} + 2\overline{u_i \partial_j \eta s_{kj}} \qquad (A.32)$$

We add $(A.31)$ and $(A.32)$:

$$\overline{u_k \frac{\partial u_i}{\partial t}} + \overline{u_i \frac{\partial u_k}{\partial t}} + U_j\left(\overline{u_k \partial_j u_i} + \overline{u_i \partial_j u_k}\right) + \overline{u_k u_j} \partial_j U_i + \overline{u_k u_j \partial_j u_i} + \overline{u_i u_j} \partial_j U_k + \overline{u_i u_j \partial_j u_k}$$

$$= -\overline{u_k \partial_i \frac{p}{\rho}} - \overline{u_i \partial_k \frac{p}{\rho}} + 2\left(\overline{u_k \partial_j \eta S_{ij}} + \overline{u_i \partial_j \eta S_{kj}}\right) + 2\left(\overline{u_k \partial_j \eta s_{ij}} + \overline{u_i \partial_j \eta s_{kj}}\right) \qquad (A.33)$$

We then obtain $(A.34)$:

$$\frac{\partial \overline{u_i u_k}}{\partial t} + U_j \frac{\partial}{\partial x_j} \overline{u_i u_k}$$

$$= -\overline{u_k u_j} \frac{\partial U_i}{\partial x_j} - \overline{u_i u_j} \frac{\partial U_k}{\partial x_j} - \frac{\partial \overline{\left(u_i u_j u_k\right)}}{\partial x_j} - \overline{u_k \frac{\partial \frac{p}{\rho}}{\partial x_i}} - \overline{u_i \frac{\partial \frac{p}{\rho}}{\partial x_k}}$$

$$+2\left(\overline{u_k\partial_j\eta S_{ij}}+\overline{u_i\partial_j\eta S_{kj}}\right)+2\left(\overline{u_k\partial_j\eta s_{ij}}+\overline{u_i\partial_j\eta s_{kj}}\right)+\text{buoyancy terms} \qquad (A.34)$$

We take the trace of $(A.34)$:

$$\delta_{ik}\left[\frac{\partial\overline{u_iu_k}}{\partial t}+U_j\frac{\partial}{\partial x_j}\overline{u_iu_k}\right]$$

$$=\delta_{ik}\left[-\overline{u_ku_j}\frac{\partial U_i}{\partial x_j}-\overline{u_iu_j}\frac{\partial U_k}{\partial x_j}-\frac{\partial\overline{\left(u_iu_ju_k\right)}}{\partial x_j}-\overline{u_k\frac{\partial\frac{p}{\rho}}{\partial x_i}}-\overline{u_i\frac{\partial\frac{p}{\rho}}{\partial x_k}}\right]$$

$$+\delta_{ik}\left[2\left(\overline{u_k\partial_j\eta S_{ij}}+\overline{u_i\partial_j\eta S_{kj}}\right)+2\left(\overline{u_k\partial_j\eta s_{ij}}+\overline{u_i\partial_j\eta s_{kj}}\right)\right]$$

$$\frac{\partial\overline{u_iu_i}}{\partial t}+U_j\frac{\partial}{\partial x_j}\overline{u_iu_i}=-2\overline{u_iu_j}\frac{\partial U_i}{\partial x_j}-\frac{\partial\overline{\left(u_iu_ju_i\right)}}{\partial x_j}-2\overline{u_i\frac{\partial\frac{p}{\rho}}{\partial x_i}}+4\overline{u_i\partial_j\eta S_{ij}}+4\overline{u_i\partial_j\eta s_{ij}} \qquad (A.35)$$

We then use chain rule:

$$2\frac{\partial}{\partial x_j}\overline{u_i\eta S_{ij}}=2\overline{u_i\frac{\partial}{\partial x_j}\eta S_{ij}}+2\overline{\eta S_{ij}\frac{\partial u_i}{\partial x_j}}$$

S_{ij} is symmetric, therefore: $S_{ij}=S_{ji}$. We switch the dummy indices i and j in $\overline{S_{ij}\frac{\partial u_i}{\partial x_j}}$:

$$2\overline{\eta S_{ij}\frac{\partial u_i}{\partial x_j}}=\overline{\eta S_{ij}\frac{\partial u_i}{\partial x_j}}+\overline{\eta S_{ji}\frac{\partial u_j}{\partial x_i}}=\overline{\eta S_{ij}\frac{\partial u_i}{\partial x_j}}+\overline{\eta S_{ij}\frac{\partial u_j}{\partial x_i}}=2\overline{\eta S_{ij}s_{ij}}$$

$$4\overline{u_i\partial_j\eta S_{ij}}=4\frac{\partial}{\partial x_j}\overline{u_i\eta S_{ij}}-4\overline{\eta S_{ij}s_{ij}} \qquad (A.36)$$

$$2\frac{\partial}{\partial x_j}\overline{u_i\eta s_{ij}}=2\overline{u_i\frac{\partial}{\partial x_j}\eta s_{ij}}+2\overline{\eta s_{ij}\frac{\partial u_i}{\partial x_j}}$$

$$2\overline{\eta s_{ij}\frac{\partial u_i}{\partial x_j}}=\overline{\eta s_{ij}\frac{\partial u_i}{\partial x_j}}+\overline{\eta s_{ji}\frac{\partial u_j}{\partial x_i}}=\overline{\eta s_{ij}\frac{\partial u_i}{\partial x_j}}+\overline{\eta s_{ij}\frac{\partial u_j}{\partial x_i}}=2\overline{\eta s_{ij}s_{ij}}$$

$$4\overline{u_i \partial_j \eta s_{ij}} = 4\frac{\partial}{\partial x_j}\overline{u_i \eta s_{ij}} - 4\overline{\eta s_{ij} s_{ij}} \qquad (A.37)$$

$$\frac{\partial \overline{u_i u_i}}{\partial t} + U_j \frac{\partial}{\partial x_j}\overline{u_i u_i}$$

$$= -2\overline{u_i u_j} S_{ij} - \frac{\partial \overline{\left(u_i u_j u_i\right)}}{\partial x_j} - 2u_i \overline{\frac{\partial \frac{p}{\rho}}{\partial x_i}} + 4\frac{\partial}{\partial x_j}\overline{u_i \eta S_{ij}} - 4\overline{\eta S_{ij} s_{ij}} + 4\frac{\partial}{\partial x_j}\overline{u_i \eta s_{ij}} - 4\overline{\eta s_{ij} s_{ij}}$$

We then have the final form of the kinetic equation for a non-Newtonian flow during transient as the following:

$$\frac{1}{2}\frac{\partial \overline{u_i u_i}}{\partial t} + \frac{1}{2}U_j \frac{\partial}{\partial x_j}\overline{u_i u_i}$$

$$= -\overline{u_i u_j} S_{ij} - \frac{1}{2}\frac{\partial \overline{\left(u_i u_j u_i\right)}}{\partial x_j} - \overline{u_i \frac{\partial \frac{p}{\rho}}{\partial x_i}} + 2\frac{\partial}{\partial x_j}\overline{u_i \eta S_{ij}} - 2\overline{\eta S_{ij} s_{ij}} + 2\frac{\partial}{\partial x_j}\overline{u_i \eta s_{ij}} - 2\overline{\eta s_{ij} s_{ij}} \qquad (A.38)$$